Part One Biosensing and Diagnosis

Nanomaterials for the Life Sciences Vol. 4: Magnetic Nanomaterials. Edited by Challa S. S. R. Kumar

ISBN: 978-3-527-32154-4

1
Nanomaterials-Based Magnetic Relaxation Switch Biosensors

Tom Lowery

1.1
Introduction

Magnetic nanoparticles or microparticles can serve as magnetic relaxation switches (MRSws) when they react with molecular targets and undergo changes in aggregation state that affect solvent magnetic resonance relaxation. Coupling this target-mediated aggregation with an appropriate detection device yields a reagent–instrument biosensor system for detecting target analytes. Since their introduction in 2001 [1], MRSw biosensors have been the subject of over 40 reports demonstrating their capability of detecting virtually any analyte in a variety of dirty, opaque samples. MRSws have been shown capable of detecting nucleic acids, proteins, enzymes, small molecules, ions, viruses and cells in solutions such as water, blood, cell lysate, urine, plasma, and serum. Due to the broad range of possible target analytes, and the capability of obtaining measurements without sample preparation, MRSw technology has remarkable potential to change the paradigm of solution-based biosensing, and thus to impact greatly on several fields of application, including medical diagnostics, environmental sensing, and homeland security.

The MRSw technology draws on the unique combination of scientific fields of nanotechnology, biochemistry, and nuclear magnetic resonance (NMR). To date, only one brief review has been published, relatively early during the development of this technology [2]. Due to the rapidly growing body of these investigations, and the interdisciplinary nature of MRSws, there is a need for a comprehensive description of the technology and summary of recent progress. To this end, this chapter provides an introduction to the relevant nanomaterials, an explanation of relevant NMR measurement techniques, a summary of the underlying theoretical physics behind nanoparticle clustering, an overview of the published MRSw research articles, and a description of portable and miniaturized magnetic resonance instrumentation. Although a sizeable body of work exists using other types of magnetic resonance contrast agents for molecular detection [3–12], this chapter will focus exclusively on MRSw biosensors.

Nanomaterials for the Life Sciences Vol. 4: Magnetic Nanomaterials. Edited by Challa S. S. R. Kumar

ISBN: 978-3-527-32154-4

1.2 Superparamagnetic Nanoparticles

The properties of nanoparticle reagents make possible the unique characteristics of MRSw biosensing. To date, all MRSw demonstrations have used some type of superparamagnetic iron oxide (SPIO) particle. The earliest iron oxide particles were utilized for localized lymph node heating over 45 years ago [13]. SPIO nanoparticles contain one or more superparamagnetic iron oxide cores composed of a mixture of magnetite (Fe_3O_4) and maghemite (γ-Fe_2O_3), which have similar magnetic properties. These iron oxide cores, which typically are less than 14 nm in diameter, are encapsulated in a hydrophilic monomer or polymer coating so as to endow water solubility [14]. When magnetite crystals are oxidized, the crystal lattice changes from the inverse spinel of magnetite to the cubic Fe(III) oxide lattice of maghemite [14]. SPIO particles are distinguished from paramagnetic particles in that their small iron oxide cores are comprised of single-domain magnetic crystals, the magnetic moments of which readily align with an external magnetic field, and this results in a microscopic dipolar magnetic field surrounding the iron crystal. Upon removal of the external magnetic field, the magnetic moments of these cores randomize, leading to a complete dissipation of the induced magnetic field [14, 15]. The magnetization and magnetic susceptibility of SPIO nanoparticles are much larger than that of paramagnetic ions and bioinorganic complexes of iron, such as ferritin [16].

Depending on the method of synthesis, SPIO particles can range in size from ~2 nm (citrate-inhibited growth), tens of nanometers (polymer-coated), to micrometers [14]. SPIO are typically categorized based on their overall diameter, which includes the metal core and organic coating [14]. SPIO particles between 300 nm and 3.5 μm are referred to as oral-SPIO because they were first used for *in vivo* imaging via oral delivery, such as the silane-coated contrast agent ferumoxsil (trade name GastroMARK®) [17]. Like most particles larger than 50 nm, oral-SPIOs contain more than one iron core per particle. Over a matter of minutes, however, a solution of oral-SPIO particles can settle due to their large size [18], which complicates their use for the aggregation-based sensing used by MRSws. In order to circumvent this, MRSw applications using oral-SPIOs have utilized surface treatments to provide adequate buoyancy to the particles, such that they do not settle. In addition, timed mixing steps with rapid measurements have been used to ensure a reproducible suspension of the particles during measurement [19, 20].

Particles which are slightly smaller than oral-SPIO particles are referred to as standard SPIO (SSPIO) nanoparticles, and have hydrated diameters of 60–150 nm. As with oral-SPIO, these particles contain more than one iron core per particle. A solution of these particles does not settle, although under certain conditions they may aggregate when placed in a magnetic field [18]—a property which is used for magnetic separations by SSPIO (examples include those produced by companies such as Miltenyi Biotech). A similar, field-dependent aggregation has also been observed for oral-SPIO [21–23], and can be used for the sensitivity enhancement of MRSw biosensors [19]. However, the application of these particles to MRSw

biosensors must be accompanied by proper controls to ensure that the observed change in signal is the result of target binding and not simply field-induced clustering.

Particles smaller than ~50 nm are known as ultrasmall SPIO (USSPIO), some of which have been developed to produce *in vivo* contrast agents such as ferumoxide (Feridex®) and ferumoxtran (Combidex®) [24–27]. Although their density is greater than that of water, their size is sufficiently small that Brownian motion keeps them suspended in solution [18, 20]. The subjection of these solutions to a magnetic field gradient does not lead to separation from solution, as it does for larger SPIO particles [18, 20, 28, 29]. Instead, the suspended particle solution behaves like a homogeneous magnetic colloid, or ferrofluid [18]. A subset of USSPIO is those that have single monocrystalline cores. Monocrystalline iron oxide nanoparticles (MIONs) typically have hydrated diameters of 10–30 nm, which are too small for magnetic grid purification.

As will be discussed below, a variety of SPIO particle sizes and particle materials have been used for MRSw assays, ranging from USSPIO to micron-sized oral-SPIO. MRSw technology was pioneered using a variant of MION [24, 30] known as crosslinked iron oxide (CLIO) nanoparticles. CLIO nanoparticles are MION nanoparticles, the polysaccharide coating of which has been crosslinked to endow a greater stability upon the particle. As with MION, CLIO nanoparticles have iron oxide cores which are between 3 and 5 nm in size, with a crystal structure of inverse spinel structure (cubic close-packed) of $(Fe_2O_3)_n(Fe_2O_4)_m$. They are surrounded by 10 kDa crosslinked dextran polysaccharide that is approximately 10 nm thick, to result in a total particle diameter of 25–30 nm [2].

One of the earliest characterizations of USSPIO nanoparticles was reported by a team led by T. Shen in the Weissleder group at the Massachusetts General Hospital (MGH), and also by a team led by C. Jung at Advanced Magnetics [17, 24, 25, 30]. The properties determined by these studies were typical of the MION nanoparticles used to create targeted CLIO nanoparticles for subsequent MRSw studies at MGH. The MION particle characterized in the original studies has been the parent particle for several different magnetic resonance imaging (MRI) contrast agent applications, including Combidex [17, 24, 25, 31–33] and many MRSw biosensors. The sizes of MION and other USSPIO iron oxide cores were measured, using transmission electron microscopy (TEM) and X-ray diffraction (XRD), as ranging between 4 nm and 10 nm, depending on the method of preparation [24, 25, 30]. A hexagonal crystal shape was also reported, which was consistent with the inverse spinel crystal structure typical of magnetite and the results of x-ray powder diffraction studies. The magnetization of these particles was 68 emu g^{-1} at room temperature and with an external field of 1.5 T. Magnetization of these particles saturated around 50 000 gauss, or 5 T; consequently, at 0.5 T the magnetization was ~60% saturated [24, 30]. When the magnetic field was switched off, no remnant field was measured from the MION, which was indicative of their superparamagnetic nature. Shen *et al.* measured the fractional weight content of iron and dextran on MION to deduce an 80 : 1 iron : dextran molar ratio, although this value would, of course, depend on the specific preparation of the MION. Both,

iron and dextran content were determined by chemical pretreatment and spectrophotometry. In solution, the MION were unimodal, with an average hydrodynamic radius of 20 nm, as determined by laser light scattering [24, 30]. When MION were placed in nonaqueous micelles, their overall diameter decreased to 8 nm, underlining the porous nature of the dextran polymer layer. Based on the crystal structure and TEM measurements of the iron core, each iron core was calculated to contain 2064 iron atoms. Accordingly, each core was calculated to have 25 ± 6 dextran molecules (10 kDa) attached [30].

Many different synthetic methods have been introduced for synthesizing superparamagnetic nanoparticles, and the reader is referred to pertinent reviews for further details [34–39]. Water-soluble CLIO nanoparticles can be synthesized using a two-step method, involving the base-induced crystallization of iron salts in the presence of a polysaccharide to form MION, with subsequent crosslinking to form CLIO [30, 32, 33]. In this method, ferric salts were stirred overnight in an acidic aqueous solution at 4 °C in the presence of dextran, which is a highly soluble, linear polysaccharide composed of D-glucose. Following the addition of ferrous salt and titrating with ammonium hydroxide to form a basic mixture, the temperature was increased to 80 °C, at which point precipitation of the MION nanoparticles occurred. Any unreacted dextran was then removed by filtration, and the dextran coating crosslinked by the addition of epichlorohydrin and aminated by reaction with ammonia [40, 41]. These series of reactions resulted in a MION particle that was coated with aminated, crosslinked dextran, referred to as an amino-CLIO. Amino-CLIO nanoparticles have an iron core diameter of 5 nm and a hydrated diameter of 25–30 nm, which is equivalent in size to a globular protein between 750–1200 kDa [2]. The surface amino-CLIO can be functionalized by attaching appropriate targeting moieties to amino groups, such as antibodies or binding proteins, using standard bioconjugation chemistry techniques.

1.3 Agglomeration-Based Sensing

The fundamental means by which magnetic relaxation switch biosensors detect the presence of an analyte is analogous to agglutination-based immunoassays. Agglutination immunoassays, which were first conceived over 50 years ago [42], detect the presence of a target analyte by using microparticles (often latex) decorated with a selective binding agent, such as an antibody. On addition of the target analyte, the functionalized microparticles undergo a transition from dispersed to agglomerated that is often detected by a change in the optical density of the solution [42, 43]. The limitations of this approach include the need to obtain a transparent sample for optical detection of the agglutination phenomenon, and low sensitivity and high interference rates due to nonspecific binding to the microparticle surfaces. For this reason, many applications that require higher sensitivity and selectivity require multiple washing steps to remove high-concentration interferents that bind, nonspecifically, any low-affinity particles [43, 44]. Unlike standard agglutination-based

assays, MRSw biosensors can be measured in opaque samples, and do not experience the same level of nonspecific binding to particle surfaces. These two distinguishing attributes arise from the advantages of the nanoparticle reagents and the non-optical magnetic resonance measurement approach; therefore, MRSw biosensor measurements can be conducted in relatively "dirty" samples, and with very few fluidic pre-processing steps [1, 2, 45–49].

A selective binding sensitivity of a nanoparticle for a desired molecular target can be achieved by the attachment of binding groups, such as antibodies or oligonucleotides, to the nanoparticle. If the binding group can bind to more than one site on a given analyte, and there are multiple binding sites per nanoparticle, the addition of an analyte to target-sensitized nanoparticles leads to a self assembly of the nanoparticles and target analytes into what has been termed nanoaggregates (Figure 1.1). In this manner, nanoparticles can be configured to switch from a dispersed state to an aggregated state due to the presence of an analyte. The basis of this transition is the tailored affinity of nanoparticle surface groups for a specific analyte. Similarly, nanoparticles can be configured to switch from aggregated to dispersed states due to the presence of analyte. As will be discussed below, a wide range of strategies have been employed by research groups to effect a transition between clustered and dispersed nanoparticles.

The transition of nanoparticles from dispersed to clusters can be quantitatively detected by measuring a change in a magnetic resonance signal, called "T_2", from surrounding water molecules. Because of the nature of the T_2 signal sensitivity, changes in the fraction of clustered nanoparticles can be detected without the separation of target-free from target-bound nanoparticles. The capability of measuring a binding phenomenon without a washing step represents a powerful advantage of MRSws over other technologies. This greatly simplifies sample handing and measurement steps, and also enables the use of extremely simple and rapid test formats.

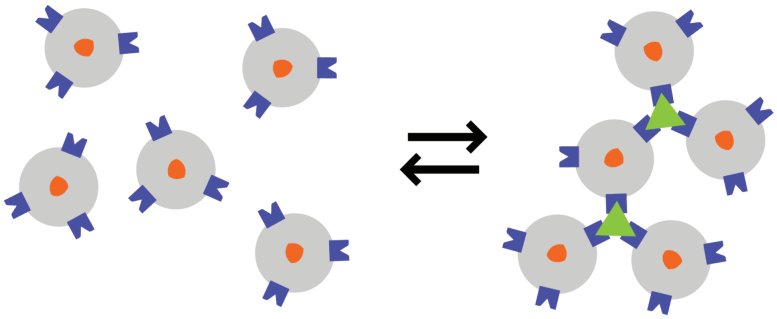

Figure 1.1 Magnetic relaxation switch biosensors are based on the magnetic resonance detection of the transition of dispersed and clustered populations of targeted nanoparticles. The targeted nanoparticles consist of a superparamagnetic iron oxide core (orange), a polymer coating (gray), and selective binding agents (blue). For one biosensor configuration, the addition of an analyte (green) leads to nanoparticle self-assembly to form nanoparticle–analyte aggregates.

1.4
T_2 Sensitivity of MRSW Particles

Understanding the connection between the T_2 signal and the agglomeration state of the nanoparticles is critical for designing MRSw systems. In the following sections, both the mechanism and measurement of T_2, and the connection between nanoparticle agglomeration and T_2, are described. This aim of this section is to introduce investigators to the fundamentals of the magnetic resonance measurement of MRSw assays, so as to better enable biosensor development and optimization.

1.4.1
Fundamentals of T_2 Relaxation

Magnetic relaxation switch biosensors require measurement of the magnetic resonance T_2 relaxation parameter of bulk water. The T_2 relaxation measurement can be used to determine the extent of particle agglomeration, and thereby the amount of analyte present in a sample. This explanation is one model for the T_2-sensitivity of water protons to the microscopic field nonuniformities created by SPIO nanoparticles. Other mechanisms, such as particle motion, also lead to spin dephasing. The results from a more complete theoretical model are presented below.

Magnetic resonance signals arise from the nuclei of water hydrogen atoms. According to the classical description of NMR, these nuclei can be thought of as having tiny spins that precess in the presence of an external magnetic field, such as that provided by a permanent magnet inside a relaxometer. The rate of precession of the nuclear spins is directly proportional to the strength of the magnetic field, by the equation:

$$\omega_0 = (1/2\pi)\gamma B_0 \tag{1.1}$$

where ω_o is the proton precession frequency (Lamour frequency) in Hz (20 MHz for 0.47 T), γ is the gyromagnetic ratio of protons (2.675×10^8 rad s^{-1} T^{-1} for protons), and B_o is the strength of the applied magnetic field. An ensemble of nuclear spins inside a magnetic field arranges into two quantum spin states of different energies. The higher energy state corresponds to spins that align against the applied magnetic field, while the lower energy state corresponds to spins that align with the applied field. As the lower energy state has a slightly higher population ($<1 \times 10^{-6}$), there is a net nuclear magnetization that points in the same direction as the magnetic field (Figure 1.2a). To detect the spins, the magnetization vectors are "tipped" into the x–y plane (Figure 1.2b), also called the "transverse plane", by means of a transient magnetic field, B_1, which is perpendicular to and smaller than the main B_o field. Such transient B_1 fields are generated by radiofrequency (RF) pulses from specialized antennae, typically called coils. Once in the transverse plane, the ensemble of spins oscillate about the B_o field (Figure 1.2c); indeed, it is this oscil-

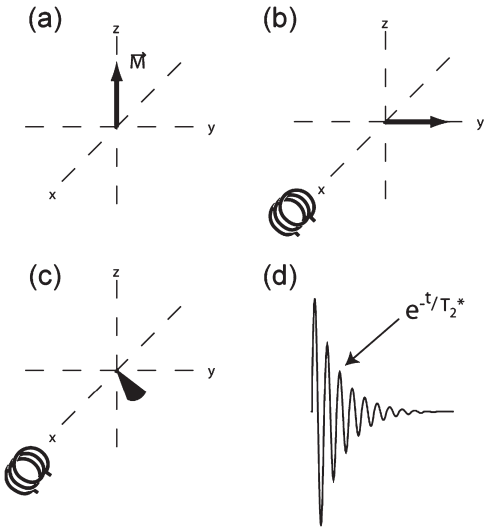

Figure 1.2 A series of schematics explaining nuclear magnetic resonance detection according to classical physics. (a) When nuclear spins are in the presence of a magnetic field, a bulk magnetization vector is present from the majority of the spins aligning with the field direction; (b) This magnetization can be detected by subjecting the sample to a radiofrequency pulse that tips the bulk magnetization vector into the x–y plane; (c) As this vector oscillates in transverse plan it decays according to T_2^* relaxation. This decay is called "spin dephasing", which is depicted by the vector fanning out; (d) Detection of the oscillating magnetic vector yields an oscillating signal that decays with a time constant of T_2^*.

lation which is detected by the RF detection coil, which is typically the same coil as that used to generate the RF pulse.

Once generated, the magnitude of the oscillating signal decays according to spin–spin relaxation, which occurs when a given ensemble of oscillating spins lose coherence, or synchronicity. This can be depicted by an oscillating vector "fanning out" over time (Figure 1.2c). A loss of spin coherence leads to a decay in the oscillating signal. A measure of the magnitude of this decay is the time constant T_2^* (Figure 1.2d).

A loss of spin coherence occurs when the spins within an ensemble experience variations in their Lamour frequencies, ω_o, during oscillation in the transverse plane. Such variations are caused not only by macroscopic inhomogeneities but also by microscopic fluctuations in the local B_o field. The contribution of macroscopic and microscopic B_o variations to T_2^* relaxation can be differentiated by specific detection sequences, as will be discussed below.

In both USPIO and SSPIO samples, microscopic variations in B_o are dominated by the agglomeration state of the particles. Measuring this contribution to T_2^* is critical for detecting the agglomeration state of particles. Because of their magnetic properties, superparamagnetic particles create local magnetic fields when in the presence of a B_o field; this in turn creates a local field "gradient", or a spatially

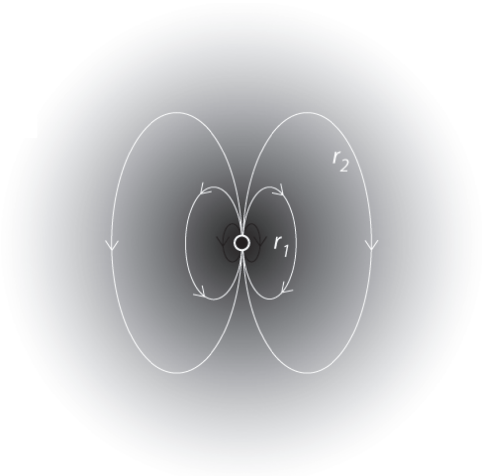

Figure 1.3 When inside a magnetic field, superparamagnetic particles generate local fields. The strength of the generated fields decreases as a function of distance from the particle, as indicated here by the spacing of the white field lines and the shading.

changing magnetic field, directly around each particle. The shape of this gradient is much like that generated by a simple bar magnet (Figure 1.3). The B_o field experienced by a given spin is the sum of the applied field and the local field generated by a particle (Equation 1.1). Spins that are near the particle, r_1, and those that are far away from the particle, r_2, precess at different frequencies, ω_1 and ω_2, respectively (Figure 1.3). Because water molecules are constantly diffusing, spins at r_1 and oscillating at ω_1 can move to r_2 and oscillate at ω_2 over the time course of signal detection. Such changes in ω_o lead to a loss of coherence, or synchronicity, between the spins within an ensemble.

The loss of spin coherence due to diffusion can be understood in terms of the property called phase. Phase corresponds to the relative positions of the magnetization vectors of spins in an ensemble. Figure 1.4a shows the magnetization vectors for two spins in the presence of the same magnetic field, such as at position r_2 (see Figure 1.3). When one of the spins transiently experiences a different magnetic field, such as diffusing from r_2 to r_1 and back to r_2 (Figure 1.3), then it undergoes a change in phase, as shown in Figure 1.4b. This change in phase arises from spins transiently oscillating at different frequencies due to changes in B_o field strengths. Because all spins in the sample are rapidly diffusing, the magnetization vectors of all spins undergo different phase shifts, leading to loss of spin coherence over time; this phenomenon is also called spin dephasing.

Spin dephasing occurs during signal acquisition, and affects the measurement (as shown in Figure 1.5). The NMR detector detects the bulk magnetization, or the sum of the magnetization vectors of each spin. When a population of spins

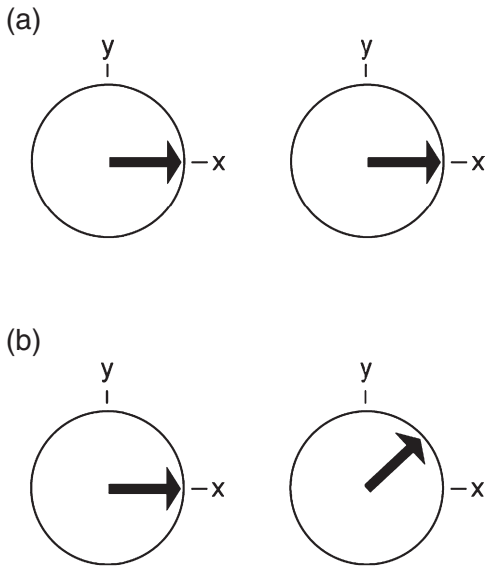

Figure 1.4 A schematic explaining the phenomenon of dephasing, or loss of phase coherence. (a) Snapshot of magnetization vectors for two spins that are oscillating at the same frequency because they are experiencing the same magnetic field. These two spins have the same phase; (b) A snapshot of these two spins after one spin has experienced a stronger field for a short time. They are still oscillating at the same frequency, but one spin has acquired a phase shift due to temporarily experiencing a different magnetic field, such as that experienced by a water molecule that has diffused past a superparamagnetic particle.

dephase, the bulk magnetization vector "fans out", decreasing the observed signal as a function of time (Figure 1.5a). However, if a sample experiences greater magnetic field variations (Figure 1.5b), then the observed magnetization vector will dephase (fan out) more rapidly, leading to a more rapid decay in the observed signal (Figure 1.5b).

1.4.2 Detecting T_2 Relaxation

Magnetic resonance signals are measured by pulse sequences, which are so named because they consist of a series of RF pulses separated by specific delays for spin evolution and signal detection. An RF pulse generates a transient magnetic field, B_1, that is perpendicular to the main magnetic field, B_o, as mentioned above ($B_1 << B_o$). The power and length of an RF pulse is tuned to rotate the bulk magnetic moment of the nuclear spins a given amount, such as 90° or 180°. The most simple pulse sequence consists of a pulse that rotates the magnetic field into the transverse plane for detection (see Figure 1.2); this is commonly referred to as a "90° pulse–detect measurement".

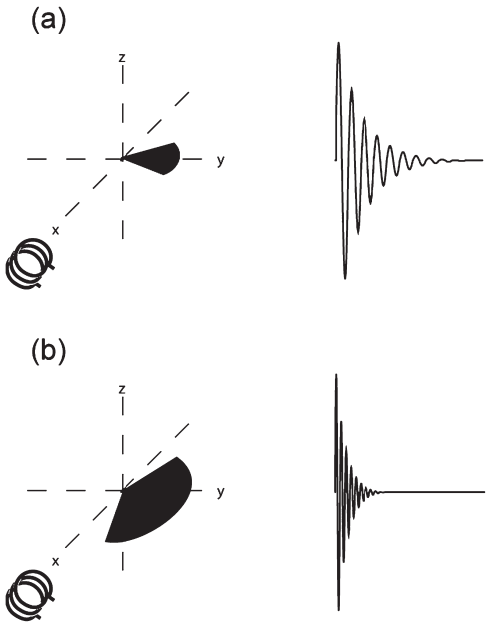

Figure 1.5 NMR signal acquisition from two samples that have (a) a long T_2 value; and (b) a short T_2 value. These two samples could be a sample of (a) disperse and (b) agglomerated MRSW particles. When the spin dephasing is more pronounced (b), the NMR signal decays more rapidly, corresponding to a lower T_2 value.

The simple 90° pulse–detect measurement can be used to measure T_2^*. As discussed above, magnetic field nonuniformities lead to nuclear spin dephasing. The amplitude of spin dephasing can be measured by determining the decay constant of the oscillating signal in the transverse plane, T_2^*, as shown in Figure 1.2d. For magnets used in most bench-top and portable relaxometers, T_2^* is dominated by variations in the applied magnetic field across the sample, which are also known as magnetic field inhomogeneities. The inhomogeneities of a magnetic field can be reported in terms of ppm, as calculated by the equation:

$$\Delta\omega_0(ppm) = \frac{1}{\left(\omega_0 T_2^*\right)} \tag{1.2}$$

where $\Delta\omega_o(ppm)$ is a measure of the inhomogeneity of the magnetic field, or relative change in homogeneity across a specific volume, ω_o is the Lamour frequency (in MHz), and T_2^* is the exponential decay rate in seconds of the magnetic resonance signal after a single 90° pulse–detect sequence. If one wishes to use T_2^* as a means to measure systems with long effective T_2 values, such as MRSw solutions, then magnets with high homogeneities (<0.1 ppm) must be used, such as

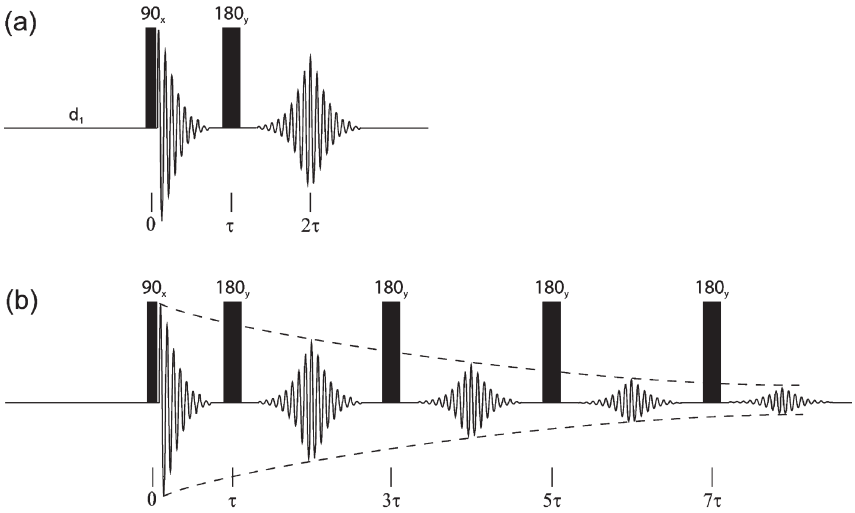

Figure 1.6 Two different MR pulse sequences for measuring T_2. (a) A spin echo sequence consists of two radiofrequency (RF) pulses: a 90° *x* phase, and a 180° *y* phase, separated by a delay τ. The echo signal appears at time 2τ. T_2 is measured by obtaining the echo signal from successive cycles using incremental values of τ. The recycle delay, d_1, is typically 1–3 s; (b) A CPMG sequence allows for much faster T_2 measurements because multiple echos are acquired in rapid succession by a series of 180° *y* phase RF pulses and signal acquisitions. T_2 measurements acquired with a CPMG sequence avoids diffusion artifacts because of the short time over which the measurement occurs.

those found in high-field superconducting magnets or large nonportable permanent magnets.

More sophisticated pulse sequences allow for the measurement of T_2 relaxation in the presence of a relatively inhomogeneous magnetic field. To do this, the contribution of magnetic field inhomogeneities to signal decay must be removed, which can be achieved using "spin echoes". The phenomenon and use of spin echos were discovered early during the development of magnetic resonance by Erwin Hahn, and later refined for rapid T_2 measurements by H.Y. Carr, E.M. Purcell, S. Meiboom and D. Gill to yield the so-called CPMG sequence [50–52]. A spin echo sequence is composed of two pulses; the first pulse rotates the spins 90°, and the second 180°. After the first pulse, the spins oscillate in the transverse plane and begin to dephase, as shown in Figure 1.5. After time τ, the fastest oscillating spins are on the leading edge of the "fan", while the slowest oscillating spins are at the lagging edge of the fan. A 180° pulse flips the spins in the transverse plane to the opposite side of the *z*-axis, switching the relative positions of the fastest and slowest spins. After time 2τ, the fastest spins catch up with the slowest, thus refocusing the magnetization vectors and the observed signal (Figure 1.6a). In order to obtain a measure of the decay constant that results from microscopic magnetic field fluctuations, or T_2, a series of spin echo sequences are run with incremented delay times, τ(typically milliseconds). Sequential scans must be

separated by a recycle delay, d_1, to allow the system to return to equilibrium as dictated by the spin-lattice relaxation time T_1 (typically 1–5 s). Fitting a plot of the maximal echo signal as a function of τ yields the time constant, T_2.

Using the spin echo sequence to measure T_2 values has two limitations. The first limitation is that any diffusion of spins during the long d_1 delay time between experiments can decrease the observed T_2 values. The second limitation is the long delay time, d_1. Because at least five datum points are necessary for a data fit, spin echo sequences can require over 20 s for the measurement of one T_2 value. A much faster and more efficient means of measuring T_2 is the CPMG pulse sequence, in which additional 180° RF pulses spaced by time 2τ are included to provide for the repeated refocusing of the echo signal. The amplitude of the echos measured between the pulses decays with the time constant T_2 (Figure 1.6b). As the time constant τ is typically less than a few milliseconds, a single T_2 measurement of several hundred echos can be completed in less than 1 s. However, one must be aware that CPMG and spin echo measurements can yield different T_2 values for some systems. Typically, CPMG sequences are sensitive to magnetic field variations that occur over periods of time less than hundreds of milliseconds, whereas spin echoes are sensitive to variations that occur over periods of time of less than seconds. One result of this difference is that CPMG T_2 measurements are independent of diffusion phenomena, while spin echo T_2 measurements are heavily dependent on diffusion, and this difference must be borne in mind when comparing T_2 values obtained by the two methods. In addition, CPMG T_2 measurements can exhibit a heavy dependence on the inter-echo delay time, 2τ. However, as will be described below, this dependence may be very useful for MRSw characterization and optimization.

1.4.3
Theoretical Model for T_2 and Nanoparticle Size

Although the use of MRSw biosensors was first demonstrated in 2001 [1], the theoretical foundation for how superparamagnetic nanoparticles affect measured T_2 relaxation rates began to take shape as early as 1991 [53]. These theory-based investigations were made possible by the early experimental observations that solvent relaxivity was a function of SPIO particle size [18]. In this early study, SPIO particles of various sizes were prepared by varying the number of iron oxide cores per particle, and the effect of ferromagnetic, paramagnetic, and superparamagnetic iron oxide particles on the longitudinal and transverse relaxivity, $R_1 = 1/T_1$ and $R_2 = 1/T_2$, respectively, was reported [18]. Subsequently, a group of theoreticians in Belgium, including Robert Muller, Pierre Gillis, Rodney Brooks, and Alan Roch, began exploring the underpinnings of magnetic, paramagnetic, and superparamagnetic particles that were used as contrast agents for MRI. The initial studies demonstrated that Monte Carlo numerical simulations of a distribution of magnetic particles surrounding by hydrogen nuclei could be used to accurately reproduce the observed dependence of R_2 on the size of iron oxide micro and nanoparticles [53, 54]. Simulations and experimental data showed that both R_2

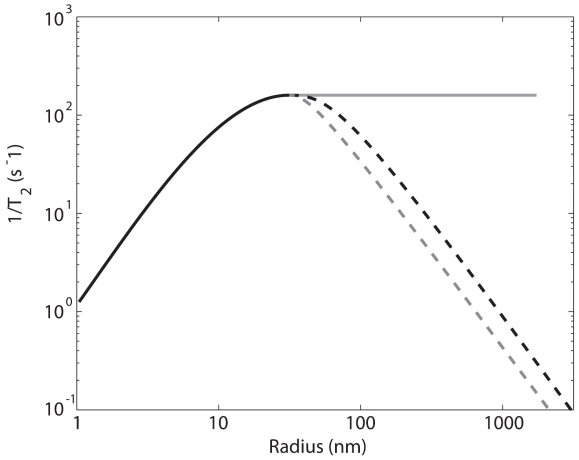

Figure 1.7 Sketch of the relationship between R_2 ($1/T_2$) and SPIO radius. In the motional averaging regime (solid dark line), R_2 increases with nanoparticle size, while in the visit-limited regime R_2 decreases with nanoparticle size (dashed lines). In the motional averaging regime, R_2 is equal to R_2^*, whereas in the visit-limited regime (also termed the static dephasing regime) R_2 no longer equals R_2^* (gray solid line). The static dephasing regime does not apply to most permanent magnet systems because R_2^* is dominated by their magnetic field nonuniformity; therefore, for portable systems R_2^* is always much larger than R_2. A unique property of the visit-limited regime is that R_2 exhibits a dependence on the inter-echo delay. The appropriate regime for a given SPIO system can be determined experimentally by measuring the R_2 and R_2^*, if using a high-field homogeneous magnet, or by measuring R_2 as a function of different inter-echo delays. These curves are a representative sketch of curves shown in Refs. [53] and [56], respectively. The exact position and curvature of the plots depends on the conditions used to generate the original curves.

and $R_2^*\left(R_2^* = 1/\mathrm{T}_2^*\right)$ increased with particle diameter until ~50 nm, whereas R_2 measured with spin echos decreased with increasing particle size, and R_2^* measured with a 90° pulse-detect reached a plateau (Figure 1.7). Subsequent experimental studies and computer simulations explored the dependence of R_2 on the concentration of dissolved iron, magnetic susceptibility, and temperature [54]. These early investigations laid the foundations for the development of a set of analytical models that accurately reproduced the dependence of transverse relaxivity on particle size, magnetization, iron concentration, temperature, and inter-echo delay for both strongly [55–57] and weakly magnetized nanoparticles [58].

According to developed theory, superparamagnetic nanoparticles are divided into categories of strongly magnetized and weakly magnetized. The boundaries between these two regimes depends on the relative magnitude of the frequency difference between nuclei at the surface of the nanoparticle and nuclei distant from the nanoparticle, $\Delta\omega$, and the inter-echo delay used in the CPMG detection sequence, τ_{CP}. $\Delta\omega$ is essentially a relative measure of the effect of the dipolar

magnetic field generated by a superparamagnetic particle on the resonant frequency of hydrogen nuclei in adjacent water molecules. When $\Delta\omega\tau_{CP} > 1$, then the particles are termed "strongly" magnetized, but when $\Delta\omega\tau_{CP} < 1$ the particles are termed "weakly" magnetized. Since, for a typical relaxometer, τ_{CP} is no shorter than tens of microseconds, $\Delta\omega$ must be less than 10^5 for the particles to be within the weakly magnetized regime. Therefore, most superparamagnetic nanoparticles used for magnetic relaxation assays are in the strongly magnetized theoretical region because $\Delta\omega$ ($\sim 1 \times 10^7$) is large compared to the inverse of achievable echo times ($1/\tau_{CP} = 10^3$). This means that the inter-echo delay is always longer than the amount of dephasing that occurs at the surface of a particle. Particles with weaker magnetizations ($\Delta\omega \sim 10^3$) induce less dephasing and are, within the theoretical regime, referred to as "weakly" magnetized.

Another characteristic of superparamagnetic nanoparticle solutions that is used to differentiate physical behavior is the diffusion time, or travel time, of water (τ_D) relative to the inter-echo time of the pulse sequence, τ_{CP}. Nanoparticle solutions are in the long echo limit when the τ_D is significantly less than τ_{CP}. τ_D can be determined by the relationship:

$$\tau_D = \frac{R^2}{D} \tag{1.3}$$

where τ_D is the time taken for a water molecule to diffuse the distance of a nanoparticle radius, R, and D is the diffusion constant of water ($10^{-9}\,m^2\,s^{-1}$). Here, τ_D can be thought of as the time taken for a water molecule to pass a hemisphere of a nanoparticle, or a "flyby" time. When τ_D is much larger than τ_{CP}, then the nanoparticle system is within the short echo limit. Typical CPMG sequences have echo times on the order of hundreds of microseconds to several milliseconds, and therefore the short echo limit cannot be approached unless the nanoparticle diameter approaches 1000 nm. The most common MRSw biosensors are within the "long echo limit" because the length of the inter-echo delays ($\tau_{CP} > 0.25$ ms) is longer than the time taken for a water molecule to diffuse pass the hemisphere of a nanoparticle (0.2–100 μs).

As the particle size of a solution of superparamagnetic particles at fixed iron concentration is increased, there is an initial increase in R_2, followed by a plateau and a later decrease (Figure 1.7). The regime on the left-hand side of the curve has been termed the motional averaging regime, the regime in the middle the static dephasing regime, and the regime on the right the visit-limited, or slow-motion regime [57]. The boundaries between the motional averaging and visit-limited regimes can be determined by generating plots such as that shown in Figure 1.7, or they can be determined by the relationship between $\Delta\omega$ and τ_D. If $\Delta\omega\tau_D < 1$, then the system is in the motional averaging regime, but if $\Delta\omega\tau_D > 1$ then the system is in the visit-limited regime. As the diameter of the particles increase in the motional averaging regime, the refocusing echos in the CPMG pulse sequence (used to measure T_2) cannot efficiently refocus the magnetization that has been dephased by the nanoparticles – hence the increase in R_2 (or decrease

in T_2). In other words, the refocusing pulses cannot compensate for increased dephasing by larger nanoparticles. The flat region of the static dephasing regime is due to R_2 being limited by R_2^*. The decreasing R_2 with increasing diameter in the visit-limited regime results in the refocusing pulses being able to refocus the dephasing caused by the nanoparticles. Also apparent in Figure 1.7 is that R_2 in the slow-motion regime exhibits a dependence on the inter-echo delay of the spin echo sequence [53].

In a homogeneous magnetic field, it is possible to determine which regime applies to a sample by comparing R_2 to R_2^*. If these values are identical, then one is in the motional averaging or static dephasing regime, but if they are different then one is in the visit-limited regime [53, 54]. This approach has been employed for determining the physical characteristics of MRSw biosensor systems [59–61]. However, as discussed above, the T_2^* of bench-top relaxometers is rarely larger than 5 ms, resulting in a lower limit for R_2^* of 200 s^{-1}. This means that, on bench-top relaxometers, R_2 will never be equivalent to R_2^* except at extremely high iron concentrations. For example, a typical solution of nanoparticles such as CLIO-47 has an R_2 of 40 $mM^{-1}s^{-1}$, so for R_2^* to equal R_2 the concentration of iron would need to exceed 5 m*M*, which is 50-fold higher than typical iron conditions. The relationship between R_2^* and field homogeneity is important to bear in mind when selecting instruments for characterizing MRSws. Fortunately, the echo time dependence of R_2 allows an easy method for determining whether one is in the motional averaging or visit-limited regime.

The conditions used to generate the analytical models that explain the dependence of R_2 on particle size were similar to the conditions used for MRSw assays. That is, the concentration of iron was held constant while R_2 was monitored as a function of nanoparticle diameter. The analytical models have been shown to accurately predict the dependence of R_2 on parameters that a biosensor designer can control, such as iron concentration, temperature, magnetic susceptibility, particle size, and particle size [54]. Interestingly, all of these parameters remain relatively constant for a given MRSw in comparison to particle size, which dominates the change in R_2. The same group which developed the analytical models was the first to demonstrate that these models could be used to explain the behavior of a system of clustering superparamagnetic particles [62]. Their experimental system consisted of superparamagnetic nanoparticles that clustered due to a change in the pH of the solution. After an initial phase that was attributed to a stabilization of the dispersed particles, R_2 was seen to increase with agglomeration until a plateau was reached prior to a decrease in R_2 with agglomeration. The shape of the R_2 response as the particles agglomerated generally matched the expected trend for the increase in average nanoparticle size, which was similar to the shape of both dashed lines in Figure 1.7. Additionally, Roch *et al*. demonstrated a general quantitative agreement between the measured and expected R_2 values. Similar exercises have since been carried out by subsequent authors to validate the qualitative nature of the T_2 response they were observing, and to determine which regime their nanoparticle assays fell within [20, 59, 61].

The similarity between the R_2 of particle agglomerates and that of spherical nanoparticles suggests that one can equate nanoparticle aggregates and spherical shapes. Even though this assumption may seem to be in contradiction with the fractal nature of nanoparticle agglomerates, the shape of the nanoparticle aggregates observed by with magnetic resonance measurements is determined by the ensemble of diffusing water molecules in solution, which can be approximated by the radius of hydration measured by light scattering. Recent studies by the group of A. Jasanoff at the Massachusetts Institute of Technology demonstrated an extension of the original outer sphere theory to nanoparticle aggregates by outlining the relationship between the parameters of the outer sphere theory and the fractal nature of nanoparticle aggregates [59]. These studies were subsequently extended by the research group at MGH, who showed that nanoparticle cluster size was inversely related to the T_2 of clusters in the motional averaging regime [61], and linearly related to the T_2 of clusters in the visit-limited regime [20], thus validating application of the outer-sphere theory to MRSws. Additionally, because the fractal dimension of nanoparticle clusters is approximately 2, the number of nanoparticles in an aggregate has been shown to be linearly related to the measured T_2 value for particles and clusters in the visit-limited regime. These observations indicate that application of the outer-sphere theory can provide useful insight on at least a semi-quantitative level into understanding and designing MRSw biosensors.

1.5 Kinetics of Magnetic Relaxation Switch Biosensors

Rapid measurements are often critical for biosensor performance and application. For MRSws, the rate of the transition between dispersed and clustered nanoparticles depends on various parameters that can be controlled for a specific set of biosensor conditions. T_2 measurements can be measured in real-time during the analyte-induced response, or at the end point of the clustering reaction. For the former case, T_2 changes as a function of measurement time and the rate of T_2 change can be correlated to a quantitative amount of analyte; for the latter case, after an incubation time T_2 remains constant as a function of measurement time, and the magnitude of T_2 can be correlated to a quantitative amount of analyte. Both measurement approaches have been used for MRSw biosensors to date.

Sample mixing and loading, as well as T_2 measurements, can be completed in tens of seconds, making sample incubation the rate-limiting step for MRSw measurements. To date, incubation times have ranged between 0 and 120 min. Although several studies have demonstrated real-time T_2 measurements immediately after sample mixing [1, 45, 63, 64], most quantitative data acquired to date has used end-point readings. In some cases, faster kinetics can be achieved by using systems that transition from clustered nanoparticles to dispersed nanoparticles [63–65]. However, for both types of assay design a significant variation in

reaction rates has been observed. A recent theoretical study conducted in the laboratory of A. Jasanoff suggested how several parameters, including particle concentration, functional group density, and ratio of particle types, can be optimized to achieve reaction rates on the order of seconds [59]. The group's simulations predicted that reaction rates could vary over three orders of magnitude within reasonable activation kinetics, biomolecular on and off rates, particle concentrations, and functionalization levels.

Shapiro *et al*. have proposed a two-step model for MRSw agglomeration, with the first step consisting of an activation of both species of nanoparticles due to the presence of an analyte [59]. Such activation results from the analyte binding to or analyte-induced modification of the particle surface. The second step consisted of agglomeration of the activated nanoparticles. These two steps are shown in Equation 1.4:

$$A + B \rightarrow A^* + B^* \rightarrow \sum A_j^* B_j^* \tag{1.4}$$

where A and B denote nanoparticles of two different functionalities, A* and B* represent activated A and B particles, respectively, and $A_i^* B_j^*$ represent an aggregate composed of *i* A particles and *j* B particles [59]. These authors assumed that the rate of the first step was much faster than that of the second step, thus causing agglomeration to be the rate-limiting step. Interestingly, for sensors that are based on nanoparticle dispersion, deactivation and dispersion are likely both to be fast steps, which explains why for some sensors much faster rates are observed for nanoparticle dispersion. Because T_2 measurements made by CPMG echos can be less than seconds, the signal acquisition is rapid compared to the first two steps, and will not significantly influence most observed reaction rates.

This two-step model was used to predict how changes in particle concentration, the number of functional groups per particle, and also the ratio between particle types, could influence the observed binding kinetics and particle size. Reaction rates for different conditions were compared in terms of an observed time constant (T_{obs}). T_{obs} is the time required for the reaction to reach 63% completion (one exponential unit). A reaction following first-order kinetics is 95% complete after $3 \times T_{obs}$, and 99% complete after $5 \times T_{obs}$. Particle concentrations of 23 n*M* (iron content 10 μg ml^{-1}), which are similar to those used for most MRSw studies, have a predicted T_{obs} value of <100 s. This suggests that these reactions should be complete in less than 10 min, which is faster than many observed reaction times. This discrepancy may arise from the number of functional groups for the experimental results being much lower than those used for the simulations. Particle concentrations as low as ~10 p*M* have predicted T_{obs} values longer than 1000 s, while concentrations as high as 0.1 μ*M* and 60 functional groups per particle have predicted T_{obs} values of 2 s. Under all reaction conditions, the optimal ratio of particle types A and B was predicted to be 1 : 1. According to these theoretical results, relatively fast reaction times should be observed for particles at concentrations >50 n*M* that have been decorated with a high number of functional groups (>50). Many MRSw nanoparticles have had much fewer functional groups on their surface, corresponding with

reaction rates on the order of several minutes. These simulations can serve as general guidelines for navigating the parameter space of MRSw biosensor design. The results of studies conducted by Shapiro *et al*. have indicated that a measurement time of less than 10 min can be achieved for most nanoparticle preparations, and that that optimized sensors may allow for single-second measurement times.

1.6 Demonstrations of Magnetic Relaxation Switch Biosensors

The two most distinguishing properties of MRSws is their breadth of application and capability to detect target analytes in opaque samples. To date, MRSws have been used to detect DNA, RNA, proteins, enzymes, small molecules, hormones, bacterial cells, ions, eukaryotic cells, viruses, and antibodies (Table 1.1). Demonstrated sample matrices include whole-cell lysates, whole blood, serum, plasma, and urine (Table 1.2). The high tolerance for opaque samples and large amounts of background substances stems from the nonoptical nature of the magnetic resonance measurement and the properties of the superparamagnetic nanoparticles. For most other biosensor methods, nonspecific binding and other surface-mediated effects lead to background interference and necessitate a washing step. The breadth of application and high background tolerance of MRSws is unprecedented among biosensor technologies.

The following sections describe the variety of examples of magnetic relaxation switch biosensor technology. The examples have been roughly grouped by analyte type, with each being described in terms of the biosensor design, reported observa-

Table 1.1 Classes of analyte detected with MRSw assay technology.

Analyte	Reference(s)
Virus	[46]
Small molecules, peptides	[23, 63, 65]
DNA, mRNA	[1, 45, 46, 66, 67]
Peroxidases	[48]
Proteases	[45, 47, 68]
Telomerase	[66]
Methylase	[46]
Hormone	[69, 70]
Ions	[60, 71, 72]
Bacterial cells	[23, 48]
Proteins	[23, 45, 49, 61, 69]
Immunoglobulins	[19]
Eukaryotic cells	[23]

Table 1.2 Conduction of MRSw assays in various media to validate potential for minimal sample processing and measurement in dirty samples.

Specimen	Analyte	Reference
Whole-cell lysates	Nucleic acids	[45]
Cell culture media	Enzyme	[47]
10% blood	Bacterial cells	[48]
2% whole blood	Enzyme	[47]
Serum	Virus	[46]
50% whole blood	Protein	[73]
50% serum	Protein	[73]
50% plasma	Protein	[73]
50% urine	Protein	[73]

tions and conclusions, and likely future directions. In all cases, the reader is encouraged to investigate the primary literature for more detail.

1.6.1 Detecting Nucleic Acids

Magnetic relaxation switch biosensor technology was invented by a team led by Lee Josephson and Ralph Weissleder at the Center for Molecular Imaging Research at MGH. In a first report, the group presented details of a biosensor that was sensitive to the presence of a 24-base pair (bp) synthetic oligonucleotide sequence [1]. The biosensor design consisted of a solution composed of a 1 : 1 mixture of two types of CLIO that differed only by the sequence of the 36-bp oligonucleotides attached to the particle surface. An average of three synthetic oligonucleotides was attached to the nanoparticles by a standard heterobifunctional crosslinker reactive with the thiol-functionalized oligonucleotide and the amino-CLIO. When the target sequence was added to this solution, a change in turbidity was observed after 3 h, and a visible brown precipitate after 16 h. The T_2 relaxation rate, measured as a function of time, was shown to have decreased from 63 ms to 45 ms within 20 min of adding the target sequence (Figure 1.8). This change in T_2 was accompanied by a change in the size of suspended particles, from 53 ± 11 nm to 215 ± 19 nm, as measured by light scattering. As with most sizing data reported for MRSws, these data were measured using photon correlation light scattering. The change in particle size and T_2 was confirmed to be a result of the specific interaction between the target DNA sequence and the nanoparticle-bound oligonucleotides by adding non-complementary oligonucleotides, which resulted in no nanoparticle clustering nor any change in T_2; by gel electrophoresis, which showed no free DNA under nondenaturing conditions; and by temperature cycling, which showed that the nanoparticle clustering was reversible upon DNA melting and annealing [1].

One common means of characterizing the transverse relaxivity of SPIO is to report R_1 and R_2. For these particles, the addition of a complementary target DNA sequence led to a change in R_2, from 75 s^{-1} mM^{-1} to 128 s^{-1} mM^{-1}, but no change in the R_1 of 27 s^{-1} mM^{-1}. A linear dependence of measured T_2 values on the amount of nucleic acid analyte was reported (Figure 1.8), which was consistent with the above-discussed observations of particle size and relaxivity [20, 61]. Josephson *et al.* were able to detect tens of femtomoles of DNA in 1 ml, and suggested that amounts as low even as attomoles might be detected. This sensitivity was realized three years later when by tens of attomoles of DNA oligonucleotides were detected in a volume of 50 µl (0.2 p*M* concentration) after a incubation time of 40–60 min and a change in T_2 of 30 ms [66]. Grimm *et al.* compared the sensitivity and dose response of their MRSws to a standard telomeric repeat hybridization assay, which was a PCR-dependent, ELISA-based photometric assay. For their 54-mer telomeric repeat test sequence, these authors showed a very tight correlation (r^2 = 0.99) and equivalent sensitivity between the two methods. Grimm *et al.* concluded that the performance of MRSws matched that of PCR-independent assays, and was within the upper range of PCR-based assays. Additionally, MRSws have advantages over other DNA assays in that they are inherently quantitative, quick and simple to run, have no requirement for a solid phase, and inherently lack the PCR-related artifacts [66].

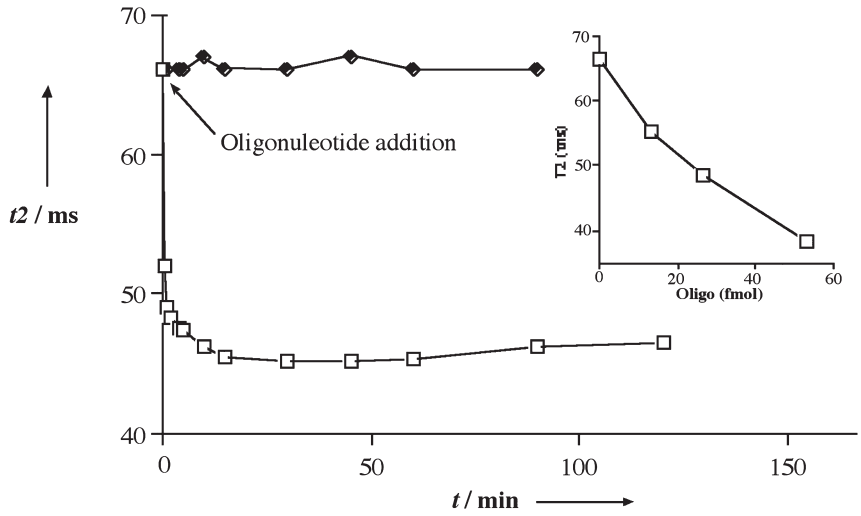

Figure 1.8 First demonstration of a magnetic relaxation switch biosensor. On the addition of femtomoles of single-stranded oligonucleotide the T_2 value was decreased by 20 ms due to nanoparticle clustering (□). No change in T2 was observed in the absence of complementary oligonucleotide (◆). T_2 values responded linearly with increasing amounts of analyte (inset). Original figure provided by Dr Lee Josephson, Center for Molecule Imaging Research, Massachusetts General Hospital, Boston, MA. Reproduced with permission from Ref. [1]; © 2001, Wiley-VCH Verlag GmbH & Co. KGaA.

Much of the early development of MRSw biosensors was pioneered by J. Manual Perez, while working in the groups of Lee Josephson and Ralph Weissleder. A follow-up study of the first report introducing the DNA MRSw sensor further demonstrated the potential for nucleic acid sensing, and also introduced the capability to detect single-base pair mismatches [45]. The DNA-functionalized nanoparticle sensors in this study transitioned from 45 nm diameter particles to 140 nm diameter clusters upon addition of complementary mRNA, with an accompanying change in T_2 of 20 ms. The change in T_2 was shown to be sensitive to single base insertions and mismatches, and to be completely eliminated for double base insertions or mismatches [45].

Perez *et al*. also demonstrated the detection of a target mRNA from a transfected green fluorescent protein (GFP) gene in various eukaryotic cell lines [45]. T_2-based measurements were shown to correlate with GFP activity for both extracted GFP mRNA and GFP mRNA directly in cell lysate after overnight incubation with the MRSw nanoparticles. The mRNA sensors were configured similarly to those previously used for DNA sensing. Two different 12 bp, thiolated oligonucleotides were attached to two different batches of nanoparticles. The target mRNA bridged the multivalent nanoparticles to induce nanoparticle assembly into clusters [45].

These initial reports on DNA-based sensing demonstrated that the addition of a bivalent biomolecular target to trivalent DNA–nanoparticle conjugates could induce nanoparticle clustering such that a change in T_2 corresponded linearly to the amount of added analyte. These initial studies also demonstrated that light-impermeable samples could be measured, and that the assay was homogeneous because it did not require a washing step.

A recent study conducted by the group of S. Pun at the University of Washington demonstrated the use of USSPIO for gene delivery [67]. These authors functionalized 10 nm USSPIO with polyethylenimine to form positively charged USSPIO that were ~24 nm in diameter. The addition of plasmid DNA led to the formation of 100 nm complexes and an increase in the T_2 relaxation time, from 600 ms to 1400 ms. The USSPIO complexation by plasmid DNA was shown to be inhibited by the addition of high salt concentrations, which disrupted the electrostatic interactions between the negatively charged DNA and positively charged nanoparticles. In this study, all measurements were obtained on a 3 T MRI scanner with a multi-spin echo pulse sequence [67]. Based on the outer sphere theory and the particle sizes, it would be expected that these particles would undergo a decrease in T_2 upon plasmid DNA complex formation; however, the nanoparticle concentration, magnetization, solution viscosity, and external magnetic field must have been such that the nanoparticles were in the visit-limited regime (Figure 1.7). The authors could have determined the cause of their increase in T_2 by obtaining T_2^* measurements of their nanoparticle solutions or T_2 measurements using different inter-echo delays. If T_2^* had been different than T_2, or if T_2 would have changed with inter-echo delay, then the visit-limited regime would have been confirmed. The USSPIO nanoparticles used by Park *et al*. were synthesized by a new formulation [36], which might also explain their unique behavior. The further characterization

of these nanoparticles, in terms of magnetic relaxation biosensing, will clarify the apparent discrepancy in the observed change in T_2.

1.6.2 Detecting Proteins

The general applicability of MRSw design introduced with DNA detection was quickly demonstrated for other types of analyte. A team led by J. M. Perez, whilst at MGH, demonstrated the capability of MRSws for measuring proteins by attaching biotinylated anti-GFP polyclonal antibodies to the surface of avidin-functionalized, dextran-coated SPIO nanoparticles. When GFP was introduced to a solution of anti-GFP decorated nanoparticles (45 nm diameter), there was a time- and dose-dependent response in the measured T_2 values. After about 30 min, however, the T_2 signal stabilized, indicating that the clustering reaction had reached completion. Concentrations of GFP as low as single nanomolar were detected with T_2 changes on the order of 10–20 ms [45].

Subsequent studies led by S. Taktak at MGH demonstrated that proteins could be detected by decorating the nanoparticles with a ligand for which a multivalent protein target had a selective binding affinity. This biosensor was created by functionalizing superparamagnetic nanoparticles with the ligand biotin, such that there were ~70 biotins per nanoparticle [61]. Addition of the tetravalent protein avidin led to nanoparticle clustering and a change in average particle size, from 30 nm to 150 nm. There was a concomitant increase in R_2, from 37 mM^{-1} s^{-1} to 132 mM^{-1} s^{-1}, which corresponded to a decrease in T_2 of 135 ms to 38 ms at an iron concentration of 0.2 mM. Taktak *et al.* extensively characterized the biophysical characteristics of their avidin MRSw system by introducing the concept of reporting analyte titrations in terms of the ratio of moles of analyte to moles of nanoparticles. According to their observations, the linear T_2 response for avidin spanned 0.4 and 1.2 avidin per nanoparticle equivalent. This approach, which relies on knowing the moles of iron atoms per nanoparticle, has been shown to be particularly useful for determining the point at which cluster formation leads to unstable aggregates [61, 69].

Taktak *et al.* reported T_2 and T_2^* measurements at 1.5 T, 4.7 T, and 9.4 T to confirm that their system was in the motional averaging regime, which was consistent with the linear dependence of R_2 on average particle size (Figure 1.7). From these data and the available theory, the group predicted that there was a decrease in cluster magnetization as the cluster size increased, and an accompanying increase in volume fraction of the clusters during agglomeration. These results were consistent with the clusters being porous fractal aggregates, as determined by other theoretical and experimental observations [59, 61]. The use of this avidin MRSw sensor for the development of new sensitivity enhancement methods is discussed in greater detail below.

The protein hormone human chorionic gonadotropin (hCG) was detected by antibody-decorated nanoparticles by a team in Michael Cima's laboratory at the MIT [69]. hCG functions as a clinical pregnancy marker, and is also overexpressed

by certain types of malignant cancers. G. Kim and coworkers used two monoclonal antibodies to generate a sandwich assay MRSw which consisted of two types of nanoparticle, each decorated with a different monoclonal antibody, mixed in a 1 : 1 ratio. The two monovalent antibodies bound to nonoverlapping epitopes on the hCG protein. Antibody–nanoparticle coupling was then conducted such that, on average, there were between 2 and 4.5 antibodies per nanoparticle. The addition of hCG to a 1 : 1 mixture of nanoparticles led to an increase in particle size as well as to a decrease in T_2. The limit of detection for this biosensor was 3.6 n*M* hCG, or 0.1 molecules of analyte per nanoparticle, after a 1 h incubation at 40 °C. As predicted by theoretical modeling [59], the nanoparticles with higher a antibody valency demonstrated greater sensitivity. These nanoparticle reagents also exhibited a time-dependent instability manifest by micron-sized cluster formation and precipitation. Interestingly, this instability was also greater at a higher antibody functionality. This same MRSw system was used to demonstrate detection of the multivalent protein A, for which there was a limit of detection of 1 μg ml^{-1} protein A, with an incubation time of 1 h at 40 °C. The limit of detection in terms of target molecules per nanoparticle was on the order of 0.1 to 1 for both hCG and protein A [69].

T2 Biosystems has demonstrated the potential for enhancing the sensitivity of a protein assay by using the hCG assay introduced by Kim *et al*. and improving its limit of detection to beyond that offered by commercial hCG diagnostic assays. Efforts aided by a fundamental theoretical understanding of agglomerative-based assays and novel signal enhancement methods provided a 3000-fold improvement in sensitivity over that reported by Kim *et al*. [74].

The demonstrations of protein detection with MRSws extended their range of application to include any biomolecular target for which an antibody is available. Because of the long history of commercial immunoassays, antibodies are available for thousands of medically relevant targets. The adaptability of MRSws to the immunoassay format will most likely enable new applications that rely on speed to obtain results, on simple sample processing, and also portability to the field of *in vitro* medical diagnostics.

1.6.3 Detecting Enzymes

Both, nucleic acid and protein sensing require a molecular binding step between the nanoparticle reagent and analyte. At an early stage of MRSw research, the range of application was extended to detect enzymatic targets, which cannot be sensed via molecular binding interactions.

The first demonstration of enzyme sensing with MRSw biosensors was made shortly after their first being reported. These studies, led by J. M. Perez, utilized two different nanoparticle–oligonucleotide conjugates which were created by functionalizing a monodisperse solution of nanoparticles with one of two complementary 18 bp strands of DNA [64]. When these two types of nanoparticle were mixed in an equimolar ratio, their oligonucleotides hybridized to create nanoparticle agglomerates that were crosslinked via double-stranded DNA (dsDNA). By design,

the crosslinking dsDNA contained a GATC sequence that could be selectively cleaved by *Bam*H1 endonuclease; indeed, the addition of *Bam*H1 to these nanoparticle clusters led to a change in T_2 from 32.3 ± 0.6 ms to 59.4 ± 0.4 ms as the nanoparticles transitioned from a clustered to a dispersed state. The increase in T_2 arose from the nanoparticles transitioning from ~350 nm clusters to ~55 nm dispersed particles [64]. This diameter-dependent T_2 response corresponded to the motional averaging regime (Figure 1.7), and has been termed a dispersive assay because analyte addition leads to agglomerate dispersion. This restriction endonuclease sensor introduced by Perez *et al.* represents the first reported dispersive MRSw assay. *Bam*H1 activity was confirmed as the source of this change in T_2 by means of gel electrophoresis on the nanoparticle reagents, and also by observing no change in T_2 when endonucleases with different selectivities were added. These results showed that, in cases where a chemical moiety exists that can be cleaved by an enzyme, that enzyme could be sensed by appropriately crosslinking nanoparticle clusters [64].

Perez *et al.* subsequently demonstrated how a simple enzyme sensor could be configured to detect other enzymatic targets, given the correct biochemical relationship. In these studies, the DNA involved in crosslinking the nanoparticles was methylated by the addition of dam methylase. The addition of a methylated-DNA-selective GATC endonuclease, *Dpn*1, then resulted in a T_2 change only when the sensor had been exposed to active dam methylase. Figure 1.9 shows that there was

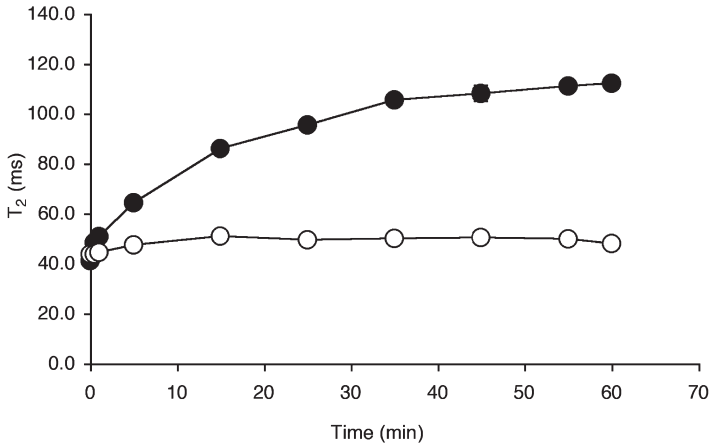

Figure 1.9 Demonstration of MRSw enzyme detection. SPIO nanoparticles were crosslinked via DNA hybridization to form nanoparticle aggregates. Aggregates that had been pretreated with methylase (●) exhibited an increase in T_2 over time after exposure to the endonuclease *Dpn*I, which selectively cleaves methylated double-stranded DNA. The increase in T_2 arose from nanoparticle dispersion. Untreated nanoparticle clusters (○) were not affected by the presence of *Dpn*I, and no change in T_2 was observed [64]. Original figure provided by Dr Lee Josephson, Center for Molecule Imaging Research, Massachusetts General Hospital, Boston, MA. Reproduced with permission from Ref. [64]; © 2002, American Chemical Society.

a change in T_2 from ~40 ms to ~120 ms over 1 h only for those nanoassemblies that had been methylated, thus demonstrating that dam methylase activity could be monitored via these nanoassemblies and *Dpn*1 [64]. Although no dose–response curve was reported for dam methylase activity, these results showed that MRSws could be configured to monitor enzymatic activity in both a direct and an indirect manner. This approach expands the types of target enzyme beyond those that can cut or cleave a crosslinking moiety. It also indicates that MRSws can be configured with coupled enzyme assays to further expand the types of enzyme and analyte that can be detected. These results also demonstrated that the internal architecture of nanoparticle clusters could be accessed by enzymes.

Shortly after the sensitivity of MRSw biosensors to endonuclease and methylase activities were reported, an analogous architecture was used to demonstrate protease detection. The same nanoparticle scaffold was decorated with either a biotinylated peptide containing the DEVD amino acid sequence, or with the protein avidin. A combination of these two types of particle led to cluster formation. Addition of the protease Caspase 3 to these clustered nanoparticles led to an increase in T_2, from 27 ms to 80 ms within 15 min [45]. In the presence of a Caspase 3 inhibitor, however, no change in T_2 was observed, thus validating the Caspase-specific T_2 response. These data further demonstrated that an enzyme activity-dependent T_2 signal could be generated by appropriately designed nanoparticle reagents [45].

Achieving true enzyme activity measurements requires a calibration curve to be obtained for a fixed reaction conditions and increasing amounts of protease. Another team at MGH, led by M. Zhao, achieved this goal and benchmarked their protease biosensor against fluorescence resonance energy transfer (FRET). Unlike the previous single-step methods, Zhao *et al*. used a two-step method for measuring protease activity [47]. The first step consisted of adding the protease of interest to a bi-biotinylated peptide that contained a cleavable amino acid sequence. After incubation at room temperature for 1 h, the second step was completed by adding the incubated sample to a solution of monodisperse avidin-coated nanoparticles. As the amount of intact bi-biotinylated peptide was inversely proportional to the protease activity, the extent of agglomeration and concomitant decrease in T_2 was, therefore, proportional to the protease activity. For the clinically relevant renin protease this assay had a similar limit of detection (69 ng ml^{-1} h^{-1} or 31 n*M* h^{-1} substrate hydrolyzed) to FRET, and had an approximately linear correlation plot with FRET over the 170 ms sampled by the T_2 measurement. If mouse whole blood was added to a volume fraction of 2% prior to signal readout, the FRET signal was completely lost, but the T_2 signal was unaffected. This demonstrated the capability for such measurements to be conducted in complex, opaque samples, and was the first reported example of a MRSw biosensor being used in diluted whole blood [47]. The fact that this two-step format did not require the direct conjugation of the peptide to the nanoparticles allowed much simplification of the reagent preparation, which in turn allowed the application of a single set of nanoparticle reagents to a broader range of protease targets.

The same two-step format was used to measure the trypsin and matrix metalloproteinase 2 (MMP-2) proteases, with limits of detection as low as $0.05\,\mu g\,ml^{-1}$ being demonstrated for trypsin. MMP-2 protease activity, which has been linked to metastasis and tumor angiogenesis, was successfully measured, using MRSws, in unpurified fibrosarcoma cell growth supernatant – conditions under which the standard MMP-2 fluorescence assay could not function [47]. This is a further example of the ability of MRSws to sample complex, turbid sample environments.

Another enzyme disease biomarker targeted by MRSw was telomerase, the activity of which may be elevated in tumor malignancies [66]. Magnetic relaxation switches were configured to monitor telomerase activity by decorating the nanoparticles with oligonucleotides that hybridized to the TTAGGG repeats synthesized by telomerase. After coupling four oligonucleotides per nanoparticle, the average nanoparticle diameter was 45 ± 4 nm. Addition of these nanoparticles to solutions containing telomeric repeats resulted in a biphasic change in T_2, with the rapid phase complete within 30 s, and the slow phase within 40–60 min. Although the exact mechanism that caused the biphasic change in T_2 was not fully characterized, the authors suggested that the nanoparticles might form pseudo-linear agglomerates along the telomeric repeats. Grimm *et al.* characterized this sensor in terms of a nucleic acid sensor that could also monitor telomerase activity [66] and, accordingly, the design provided an indirect means of measuring enzyme activity.

On realizing that enzyme activity could also be sensed by means of activating surface groups on nanoparticles to facilitate particle agglomeration, two different groups took this approach for measuring enzymes. In the first report, made by J. M. Perez at MGH, the activities of two different peroxidases – horseradish peroxidase (HRP) and myeloperoxidase (MPO) – were measured. The latter of these peroxidases has been shown to play a role in atherosclerosis and inflammation [75]. In order to detect these enzymes, either dopamine (for HRP) or serotonin (for MPO) was attached to create SPIO nanoparticles that could act as electron donors to the enzyme-catalyzed reduction of H_2O_2. After functionalizing the SPIO, each solution of nanoparticle reagent was monodisperse with a diameter of 50 nm and a ratio of ~40 reactive groups per particle. The reported R_1 was $25.8\,mM^{-1}\,s^{-1}$, and R_2 $67\,mM^{-1}\,s^{-1}$. In both cases, the peroxidase-catalyzed reduction of H_2O_2 converted the phenol group on dopamine or serotonin to a radical, which led to a radical-based crosslinking of the nanoparticles and the formation of nanoassemblies. Incubation with $0.9\,units\,\mu l^{-1}$ HRP for 2 h resulted in an increase in the diameter of dopamine-coated nanoparticles, from 50 nm to 440 nm, and a concomitant change in T_2 by 30 ms in a dose-dependent manner at 1.5 T. The MPO concentrations, which were as low as $0.003\,U\,\mu l^{-1}$, were measured in a MPO titration over one order of magnitude enzyme concentration and a range of change in T_2 between 20 ms to 300 ms at 1.5 T. At 0.5 T, the HRP sensor had a limit of detection of $0.1\,U\,ml^{-1}$, and a change in T_2 of 32 ms after a 2 h incubation at 4 °C. When H_2O_2 was not present, or a peroxidase inhibitor was added, there was no change in T_2 or nanoparticle cluster size, which indicated that the aggregate formation

was indeed due to peroxidase activity [75]. These two MRSw sensors represented the first example of agglomerative format sensing enzyme activity, and the first example of a covalently crosslinked nanoparticle assembly.

A similar approach was used by a collaborative group at MIT, the Brigham & Women's Hospital in Boston, the University of California at San Diego, and the Burnham Institute. This group, which was led by Todd Harris of the MIT, used an approach which differed from that of Zhao *et al.* to measure MMP-2 activity [68]. Rather than detecting MMP-2 by monitoring its proteolysis of a divalent peptide that has been activated to enable nanoparticle crosslinking, Harris *et al.* decorated two types of nanoparticle coated with biotin or avidin with a cleavable peptide attached to polyethyleneglycol (PEG). The bulky PEG groups inhibited binding between the biotin and streptavidin. The addition of MMP-2 led to cleavage of the peptide linker that attached PEG to the nanoparticles, thus exposing the biotin and avidin coatings so that the nanoparticles could self-assemble into clusters [68]. This indirect agglomeration approach was analogous to that used for detecting peroxidases, namely that the nanoparticle surface groups are activated by the presence of a target enzyme to facilitate particle agglomeration. Harris *et al.* reported a limit of detection of 170 ng ml^{-1} (9.4 U ml^{-1}) and a T_2 change of 150 ms at 4.7 T after a 3 h incubation. Their dispersed nanoparticles were 50 nm in diameter prior to coating with the PEG-peptide, and could be separated magnetically, which indicated that they were indeed different in nature to those used by Zhao *et al.* The MMP-2 cleavable peptide was eight residues long, and PEG chains of 2 kDa, 5 kDa, 10 kDa, and 20 kDa were tested. PEG sizes below 10 kDa did not inhibit biotin–avidin-mediated particle agglomeration in the absence of MMP-2 [68]. The sensitivity of this sensor was within the concentration range of MMP-2 typically found in tumor cells.

These demonstrations of enzyme detection showed not only the feasibility of detecting enzyme activity in both direct and indirect ways, but also the architectural flexibility of MRSws that would in turn allow designers to tailor these nanoparticle assays in a specific manner. Although, to date such flexibility has enabled the broad application of MRSws, as their development continues it is most likely that such flexibility that will lead to not only a wide range of applications but also excellent performance and sensitivity.

1.6.4
Detecting Viruses

One of the most impressive applications of MRSws has been the detection of the herpes simplex virus (HSV-1) and adenovirus (ADV) [46]. Due to the multivalent nature of these analytes, extremely low concentrations of virus could be detected in serum; in fact, a limit of detection as low as five viral particles in 10 µl was achieved, which is subattomolar in terms of viral concentration. These viral sensors were constructed by decorating superparamagnetic nanoparticles with monoclonal antibodies by means of a protein G coupling method. The monovalent antibodies bound selectively to coat proteins on the surface of either HSV-1 or ADV. The

addition of virus lead to a change in particle dispersity and size, from a monodisperse solution of nanoparticles with 46 nm diameter to a polydisperse solution containing both 46 nm particles and particles of up to 550 nm, as measured by light scattering. The aggregate size of 550 nm was consistent with a superassembly of nanoparticles and HSV or ADV viruses, as the ADV virus is ~80 nm in diameter [76] and the HSV-1 virus ~125 nm in diameter [77]; large aggregates were observed using atomic force microscopy (AFM) [46]. The addition of virus to the nanoparticle sensors led to a change in T_2 of up to 45 ms over the course of 100 min. For HSV-1, the limit of detection was 100 viral particles per 100 µl, and for ADV it was five viral particles per 10 µl. In both cases, the T_2 values were measured at 1.5 T. On a commercial instrument at 0.47 T, a similar dose and time-dependent response in T_2 was observed following the addition of viral particles [46].

In their report, Perez *et al.* noted that MRSw biosensors offered several advantages over current PCR-based viral detection methods. These included speed of obtaining results, ease of use, no requirement for enzymatic amplification, and a greater robustness. These attributes of MRSw biosensors distinguish them from many diagnostic and biosensing technologies. The most significant conclusion of the viral-based sensors has been that an increased target valency can provide greater sensitivity, a hypothesis which was later expanded upon by Hong *et al.* at MGH to provide means of increased sensitivity [20].

1.6.5 Detecting Small Molecules

Although the multivalency of viral targets provided an extremely high sensitivity for target quantification, small-molecule targets – unlike viral targets – are not multivalent. In fact, a major challenge exists to design molecule-affinity agents (e.g., antibodies) to attach in even a bivalent fashion to many small molecules. Despite this limitation, agglomeration-based assays can be configured to detect monovalent analytes by means of a competitive–dispersive format. In this case, a bivalent or multivalent binding agent is used to cluster nanoparticles that have been decorated with a derivative of the target small molecule. If the desired small molecule is present in the sample, it will compete with the modified nanoparticles from the multivalent binding agent, leading to dispersion of the nanoparticles in an amount which is proportional to the concentration of the target.

The first demonstration of a MRSw capable of detecting small molecules was made by Tsourkas *et al.*, where the D stereoisomer of phenylalanine (D-Phe) was selectively detected with background L phenylalanine (L-Phe) [63]. This report was also the first example of a nonenzymatic dispersive MRSw biosensor assay. The biosensor was capable not only of detecting a small molecule but could do so in a stereoselective manner; that is, it could distinguish D-Phe from L-Phe. Tsourkas *et al.* accomplished this by decorating superparamagnetic nanoparticles with a derivative of D-Phe in a manner that conserved the stereochemistry of D-Phe, and loaded the particles with 15 D-Phe per nanoparticle [63]. The addition of a bivalent antibody that binds D-amino acids (anti-D-AA) led to nanoparticle clustering. The

subsequent introduction of free D-Phe led to displacement of the antibody–nanoparticle complex and a dispersion of the clustered nanoparticles. For the conditions sampled, the T_2 changed by more than 100 ms for 500 μ*M* D-Phe and by about 10 ms for 5 μ*M* D-Phe. The group reported a limit of detection of 0.1 μ*M* and a coefficient of variation (CV) of <5% [63]. The kinetics of this sensor was relatively rapid (Figure 1.10), which was in general agreement with kinetic theory for dispersive assays [59]. Figure 1.10 also shows that almost two orders of magnitude in dynamic range were achieved for this MRSw. Additionally, interference studies showed that the cross-reactivity to L-Phe was 0.075% [63]. As with all MRSw biosensors, the selectivity of the MRSw was determined by the selectivity of the binding agent, which was anti-D-AA antibody in this case.

The competitive–dispersive format was used for three other small-molecule MRSws used to measure glucose, the hemagglutinin (HA) peptide, and folic acid [65]. For glucose, the nanoparticles were decorated with two glucosamine hydrochlorides and pre-complexed with the glucose-binding protein, concanavalin A. The addition of glucose led to a quantitative change in T_2 of over 40 ms within 50 min, using a kinetic reading, and a limit of detection of <50 mg dl^{-1} for glucose. For the detection of the influenza HA peptide, the nanoparticles were functionalized with HA peptide and pre-clustered with anti-HA antibody. This sensor had a T_2 change of >150 ms over a time of 100 min, and a limit of detection of <50 n*M* HA. The folic acid biosensor consisted of nanoparticles decorated with folic acid, and an anti-folic acid antibody that pre-clustered the nanoparticles. The addition of folic acid led to T_2 changes over 120 ms with reaction completion times of almost 20 min and a limit of detection of <3 n*M* [65].

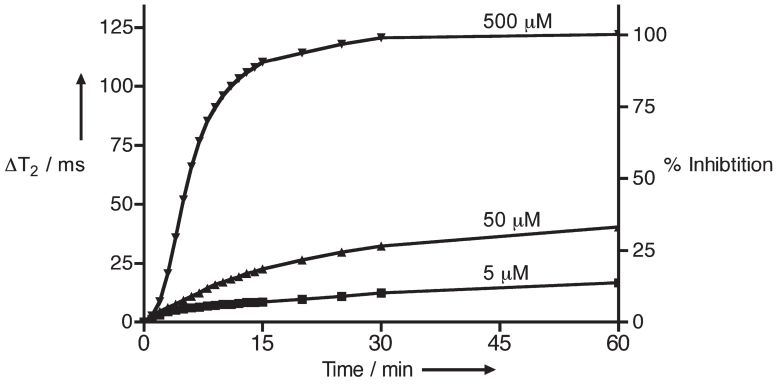

Figure 1.10 A stereoselective, small-molecule, dispersive magnetic relaxation switch biosensor. The addition of D-Phe to a solution of D-Phe-functionalized CLIO nanoparticles and antibody that binds D amino acids (anti-D-AA) led to a dispersion of the antibody–nanoparticle complex as a function of time. The rate and magnitude of the change in T_2 increased with increasing amounts of D-Phe [63]. Original figure provided by Dr Lee Josephson, Center for Molecule Imaging Research, Massachusetts General Hospital, Boston, MA. Reproduced with permission from Ref. [63]; 2004, © Wiley-VCH Verlag GmbH & Co. KGaA.

A comparison of these three small-molecule assays demonstrates the wide range of assay performance that can be achieved with MRSw biosensors. The HA assay was 80-fold more sensitive than the glucose assay, while the folic acid assay was 1000-fold more sensitive than the glucose assay [65]. Although these authors did not offer any explanation for these differences in assay performance, the variation further confirmed that the flexibility in MRSw design could be used to tailor biosensors for specific diagnostic applications. The characteristics of the folic assay were surprisingly similar to the commercial diagnostic assay for folic assay, thus validating the capabilities of this technology to meet commercial specifications [78].

The primary motivation of Sun *et al.* was to demonstrate the reversible nature of MRSws. This was achieved by containing the nanoparticle sensor solution inside semipermeable Spectra/Por tubing. Increasing and decreasing the amount of analyte, by altering its concentration in the surrounding solution, led to a corresponding change in the nanoparticle agglomeration state. Due to the membrane pore size, the nanoparticles could not diffuse across the membrane, whereas the small-molecule analytes could diffuse. In the case of the glucose sensor, the concentration of glucose was cycled six times, and this was reflected in the corresponding changes in T_2 values [65]. The reversible nature of these three sensors was made possible by the equilibrium that can exist between the dispersed and clustered nanoparticles, due to the binding characteristics of the functionalized nanoparticles and binding protein or antibodies.

These types of sensor show great promise for applications that require the continuous monitoring of target analyte levels, such as real-time environmental sensors or implantable sensors [65]. The potential for reversible sensing for implantable MRSws was introduced by the laboratories of Michael Cima and Robert Langer, using the protein biosensor for hCG and a polydimethylsiloxane (PDMS) device. The PDMS unit was designed to contain the nanoparticle reagents between two polycarbonate membranes, each of which had 10 nm pores that allowed passage of the hCG target but contained the nanoparticle reagents. The feasibility of this device for real-time sensing was confirmed by observing changes in T_2 inside the reservoirs due to changes in hCG levels in the surrounding solution, by means of MRI [70]. Subsequent studies with this device should demonstrate its use for detecting *in vivo* circulating biomarkers. In this respect, studies conducted by Daniel and coworkers have demonstrated the unique potential of MRSws in applications that require continuous monitoring. Given the appropriate instrumentation, applications can be envisioned where implanted MRSw devices are measured in a simple, portable format. Indeed, such instrumentation and applications are currently under development at T2 Biosystems and in the laboratories of both Michael Cima and Robert Langer.

1.6.6
Detecting Ions

The capability of extending the possible target analytes for MRSw biosensors to ions has been demonstrated by two ingenious experiments, both of which have

used the same general approach. This consisted of separating selective ion-binding moieties between separate nanoparticles, such that the presence of the target ion led to self-assembly of the ion-binding groups and concomitant nanoparticle agglomeration.

The first demonstration of ion detection was made by a team at the MIT in Alan Jasanoff's laboratory, led by T. Atanasijevic [60, 71]. Atanasijevic and colleagues used the reversible calcium-dependent protein–peptide interaction of the calmodulin protein and a calmodulin-binding peptide to endow calcium-dependent agglomeration upon superparamagnetic iron oxide nanoparticles. Streptavidin-coated nanoparticles (from Miltenyi Biotech) were decorated with either the calmodulin protein or with one of the two calmodulin-binding peptides, the kinase M13 peptide or kinase RS20 peptide. These nanoparticles were significantly different in terms of size and relaxivity from those used by the teams at MGH, having an iron oxide core size of 10 nm, a Fe_2O_3 content of 50% prior to protein conjugation, and with a distribution of average diameter of between 20 nm and 100 nm after conjugation to the targeting groups. In addition, because of their larger size and iron content, their R_2 was much higher at 410 mM^{-1} s^{-1} [60, 71].

The addition of calcium to a mixture of the calmodulin-functionalized nanoparticles and kinase-peptide-functionalized nanoparticles led to an increase in the average nanoparticle diameter by a factor of two, and an increase in T_2 from 27 ms to 50 ms [60]. The increase in T_2 upon cluster formation arose from the bulk of the nanoparticles being in the visit-limited regime, or the right-hand side of the T_2 versus diameter curve in Figure 1.7. This was supported by the observation of echo-time dependence of the measured T_2 values and by the authors' calculations [60].

The addition of a calcium chelator (e.g., EDTA) reversed the biosensor reaction and caused the calcium-clustered nanoparticles to disperse. As expected, reaction rates for nanoparticle dispersion were much faster than those for nanoparticle agglomeration, the latter requiring an incubation time of up to 60 min [60, 71]. The team led by T. Atanasijevic elegantly showed that the calcium concentration range over which the sensor responded could be tuned by altering the affinity of the particle-attached binding groups. The mid-point of the response curve, or EC_{50}, for wild-type calmodulin was 1.4 μM, while that for a variant of calmodulin was 10 μM. The total response range for the former was 0.1–1.0 μM, which spans typical *in vivo* calcium concentrations, and that for the latter was 1–100 μM. These two sensors could be combined to achieve an optimal dynamic range, sensitivity, and selectivity for a given application [60, 71].

A more general approach for ion detection with nanoparticles was introduced by S. Taktak in the Josephson laboratory at MGH [72]. Taktak *et al.* showed that the surface chemistry used for ion-selective electrodes could be adapted for use with MRSw biosensors. The group targeted CLIO nanoparticles by functionalization with diglycolic anhydride, which complexes Ca^{2+} at molar ratios of 2 : 1 and 3 : 1. Because calcium can induce the self-assembly of multiple diglycolic anhydride moieties, the addition of Ca^{2+} to the targeted nanoparticles led to cluster formation and a decrease in T_2, from 200 ms to 50 ms for the lowest concentration

of nanoparticles used by Taktak *et al.* As has been shown for the avidin protein biosensor, the calcium concentration range over which there was a T_2 response could be tuned by changing the concentration of nanoparticles. The addition of K^+, Li^{2+} and NH^{4+} did not elicit a change in T_2, but the addition of Mg^{2+} led to a change in T_2 which was similar to that for Ca^{2+}. This was a result of the cross-reactivity of the chelating group attached to the nanoparticles. When Ca^{2+} was added to the targeted nanoparticles in the presence of EDTA, no change in T_2 was observed, consistent with a Ca^{2+}-dependent T_2 response. The addition of EDTA to Ca^{2+}-induced clusters led to a dispersion of the clusters, and exhibited the reversible nature of this assay system. Taktak *et al.* suggested a range of chelating groups used by ion-selective electrodes that could be adapted in a similar manner to create MRSw biosensors that were sensitive to magnesium and copper [72]. This approach to ion sensor design greatly expands the range of possible target ions for MRSw biosensors due to the available chemistries used for electrochemical ion detection. Despite the commercial availability of many ion-detection technologies, the ability to detect ions with MRSw not only enables the creation of more sophisticated *in vivo* biosensors [72] but also expands the available test menu for *in vitro* biosensing.

1.6.7 Detecting Cells

One of the most recent developments in MRSw technology has been the demonstration of a capability for cell detection. This can be achieved either via indirect means, such as detecting nucleic acids or excreted biomarkers which are associated with the presence of a cell type, or by direct means, such as cell staining. Many indirect cell detection methods, including molecular testing such as PCR and immunoassays, have moderate turn-around times and costs. In contrast, direct cell detection methods, such as cell culture or cell sorting, may have slow turn-around times and high costs [79]. MRSw-based indirect and direct cell detection would allow for a low-cost, rapid turn-around time quantitative cellular testing. Whilst indirect cell detection could be achieved using many of the assays discussed above, two different groups have recently extended the use of MRSws to direct cell detection. In both cases, biomarkers expressed on the surface of the desired cell were targeted with appropriately decorated superparamagnetic nanoparticles.

The first group to report cell detection was that of J.M. Perez, at the University of Central Florida. In these studies, the group targeted the organism *Mycobacterium avium paratuberculosis* (MAP) by conjugating anti-MAP antibodies to the surface of superparamagnetic nanoparticles that were 70 nm in diameter, and had an R_2 of 320 $mM^{-1}s^{-1}$ [48]. These characteristics were much more similar to those employed by A. Jasanoff's group than by the Josephson and Weissleder groups at MGH. The titration of these particles with MAP cells led to larger changes in T_2 at lower MAP concentrations than at higher MAP concentrations. The maximum observed change in T_2 occurred at 6–8 ms after incubation times of 30–60 min at 37 °C. Although this change in T_2 approaches the run-to-run precision limit

observed by another research group [19], the reported limit of detection was 40 colony-forming units (CFU) in 10 µl of milk, and 40 CFU in 20 µl of blood [48].

The nature of the response curve observed by the authors was unlike any previously reported response curves. MRSw response curves typically approach a change in T_2 of zero as the concentration of the target decreases. For this sensor, the change in T_2 approached a maximum as the concentration of analyte approached zero. In order to explain this abnormal binding curve, the authors hypothesized that the change in T_2 was derived from a mechanism which was different than that of nanoparticle agglomeration. According to their hypothesis, the change in T_2 was a function of the proximity between superparamagnetic nanoparticles on the surface of the target cells. Accordingly, at high cell concentrations, the nanoparticles were distributed between many cells, thereby having a more distant inter-particle proximity. In addition, at low cell concentrations the nanoparticles were distributed between only a few cells, and thus had a close inter-particle proximity. Although the group validated the specificity of their observed T_2 response to the desired target cell, they failed to conduct any independent tests and controls to validate their proposed mechanism for cell detection. Consequently, further investigations will be required to confirm the source of these unprecedented T_2 response curves.

More recently, a group in the Weissleder laboratory reported the detection of intact whole cells with MRSw biosensors; these included bacterial cells from *Staphylococcus aureus* and a variety of mammalian cells. The detection of *S. aureus* was achieved by derivatizing nanoparticles with vancomycin, which binds to peptide moieties on the bacterial cell wall. Following a 15 min incubation of the vancomycin–nanoparticles with increasing amounts of *S. aureus* (from 10^0 to 10^3 cells), a linear dose–response curve with a change in T_2 of 30 ms was observed [23]. The group also reported a limit of detection of 10 CFU in 10 µl, and verified that the nanoparticles were indeed attaching to the cell surface by using TEM and energy dispersive X-ray spectrometry (EDS). This observation, in combination with a fairly extensive set of controls, indicated that the T_2 sensitivity arose from a vancomycin-dependent interaction between the nanoparticles and the cell surfaces [23].

Lee *et al.* also demonstrated the detection of mammalian cells and cell biomarker profiling. For this, mouse macrophages were detected via a multistep method that consisted of incubating the cells with fluorescein-conjugated, dextran-coated nanoparticles. Following a 3 h incubation at 37 °C to allow the macrophages to take up the dextran-coated nanoparticles, the nanoparticle-labeled cells were separated from any unbound nanoparticles by multiple washing. The resultant solution, after calibration with a hemocytometer, was used to determine the limit of detection for nanoparticle-labeled mouse macrophages; this proved to be a single cell in 10 µl, or 100 cells per ml. This multistep approach differed from the method used to detect *S. aureus*, in that the unbound nanoparticles were separated from the cell-immobilized nanoparticles. A similar multistep approach was used to profile different types of cancer cell by means of various antibody-targeted nanoparticles [23]. Although mammalian cell detection required the inclusion of washing

steps to remove any free magnetic nanoparticles, the application of tailored fluidic and separation methods will probably permit the necessary washing steps required for apparent single-step mammalian cell detection.

Although cells can be detected with MRSws via many secondary markers, cell detection via direct surface binding will undoubtedly broaden the "menu" of available tests so as to include very powerful methods such as profiling cellular expression pathways. Ultimately, many of these should enable the use of low-cost and portable applications for circulating tumor cell analysis, as well as other diagnoses that currently are possible only by utilizing cell-sorting technologies.

1.7 Methods Development

Although much of the available MRSw-related literature has demonstrated the versatility of the technology in detecting a wide range of analytes in many sample types, a subset has introduced new methods of reagent preparation and characterization, biosensor configuration, and relaxation rate measurements; these various methods are detailed in the following sections.

1.7.1 Reagent Synthesis, Preparation, and Characterization

An understanding of the physical characteristics of a nanoparticle system can be critical for the successful design of an MRSw system. During their early studies, both Shen and Jung and the coworkers relied on TEM measurements and knowledge of the iron oxide crystal form in order to determine the number of iron atoms per nanoparticle iron core (this is also referred to as the nanoparticle core weight) [17, 24, 25, 30]. Later studies performed by F. Reynolds at MGH led to the introduction of a simpler method for determining the nanoparticle core weight which used viscosity measurements and light scattering. Four parameters were used to determine nanoparticle core weight:

- The partial specific volume, as determined by a range of viscosity measurements.
- The volume of a single nanoparticle, as determined by diameter measurements with light scattering.
- The weight per volume of nanoparticles.
- The weight per volume of iron [80].

This method was easier to implement than TEM due to its use of more common laboratory equipment and faster turn-around time. Because the CLIO core weight depends on the conditions used in nanoparticle synthesis, it is important to determine the core size for new nanoparticle formulations. Knowledge of the nanoparticle core weight is necessary when calculating the average number of functional groups per nanoparticle, with cores sizes of 2000 and 8000 irons atoms per core having been reported [30, 80].

Another essential component when designing MRSws is the attachment of an appropriate targeting group, so as to endow proper binding selectivity and sensitivity upon the nanoparticles. Because the iron oxide nanocrystal is entrapped within an aminated polysaccharide coating, many common chemical crosslinking strategies can be employed. However, a specific bioconjugation method has been shown to greatly influence the performance of targeted SPIO nanosensors by altering the number and nature of the targeting groups per nanoparticle [81]. Several different types of bioconjugation strategies have been used to activate the nanoparticles. For example, a team led by E. Y. Sun demonstrated the use a CLIO variant termed a magnetofluorescent nanoparticle, which consisted of two fluorescein isothiocyanate (FITC) molecules attached to amino-CLIO nanoparticles, to demonstrate the rapid development of nanoparticle libraries. For these particles, the R_1 was $21\,mM^{-1}s^{-1}$ and R_2 $62\,mM^{-1}s^{-1}$, while the FITC absorbed at 494 nm with an extinction coefficient of $73\,mM^{-1}cm^{-1}$ [82]. Small molecules were attached via a variety of reactive handles to the ~62 free amines per nanoparticle. The small-molecule reactive handles included anhydride, amino, hydroxyl, carboxyl, thiol, and epoxy. Each of the resulting conjugates had unique functionality in terms of MRSw biosensor response and macrophage uptake, demonstrating that the specificity and selectivity of a nanoparticle conjugate is determined by the surface functionality [82]. Other crosslinkers that have been to date used include Pierce Biotech (Rockford, IL, USA) heterobifunctional crosslinking agents such as *N*-succinimidyl 3-(2-pyridyldithio)-propionate (SPDP) and *N*-succinimidyl-*S*-acetylthioacetate (SATA), generic activating and crosslinking agents such as succinimidyl iodoacetate, 1-ethyl-3-[3-dimethylaminopropyl]carbodiimide hydrochloride (EDC or EDAC), *N*-hydroxysulfosuccinimide (Sulfo-NHS), and antibody-specific coupling reagents such as protein G. In another series of studies, a team led by E.Y. Sun demonstrated the use of azide-alkyne reactions (known as "click chemistry") for the attachment of targeting groups. Sun's group demonstrated that stable alkyne- or azido-functionalized CLIO nanoparticles could be generated for click chemistry attachment to a variety of appropriately functionalized small molecules [83]. Unfortunately, the details of bioconjugation methods are beyond the scope of this chapter; thus, the reader is referred to the original data (as cited) and to more comprehensive sources [84].

Regardless of the specific coupling method used, a number of critical issues must be considered in particle design. These include the activity and number of targeting groups attached on each nanoparticle – an issue was explored by a team led by D. Hogeman at MGH. In these studies, it was shown that nonselective oxidative coupling of the protein transferrin led to an inferior biosensor performance when compared to that coupled with the heterobifunctional linker, SPDP [81]. The SPDP linker led to a fourfold increase in the number of transferrin molecules per nanoparticle, and also preserved the activity of the transferrin protein, leading to an increased binding affinity for their cellular target. The reduced affinity of transferrin when coupled to nanoparticles via oxidative coupling most likely arose from the nonselective nature of the coupling, which may

lead to cross-reactions. Directed coupling with SPDP led to increased affinities and increased binding densities, as had been shown previously for other applications [81]. The increased affinity and valency of the particles led to a 16-fold increase in the performance of the nanoparticle sensor for cell internalization. Although these studies focused on targeting superparamagnetic nanoparticles for cell encapsulation with endosomes, the dependence of performance on the bioconjugation method may be generalized for nanoparticle-based sensors [81]. Similar observations were made for a cell-targeted biosensor that used multivalent-RGD-decorated nanoparticles to bind cell-surface integrin proteins [85].

Several other reports have been made of the methods used for coupling targeting groups to polymer-coated, superparamagnetic nanoparticles. Some of these have utilized bifunctional nanoparticles, such as fluorescently labeled CLIO nanoparticles, to conduct parallel synthesis and high-throughput screening (HTS) on large numbers of nanoparticles for cell recognition applications [86]. Robotic systems have also been used to conjugate 146 different small molecules (<500 Da) to fluorescently functionalized CLIO nanoparticles [87], with the average coupling ratios being 60 small molecules per nanoparticle. These nanoparticle conjugates were also screened for eukaryotic cellular uptake, thus demonstrating that nanoparticle surface modification can target nanoparticles not only to different cell types but also to different physiological states of the same cell type [88].

1.7.2 Measurement and Sensitivity Enhancement Methods

A variety of reports have introduced new methods for measuring MRSw assays to improve measurement accuracy and sensitivity. One such report, made by a team led by S. Taktak, utilized a biotin–avidin model system to examine the physical characteristics of the MRSw biosensor system [61]. The model system was created from biotinylated nanoparticles that agglomerated in the presence of the tetrameric protein avidin. Upon the addition of avidin, the T_2 changed from 100 ms to 40 ms after incubation at room temperature for 1 h. Taktak *et al.* showed that the overall average cluster size increased linearly with the addition of avidin, and that the observed R_2 depended linearly on the average particle size [61]; these findings were similar to previous results which demonstrated avidin-coated particles and a bi-biotinylated peptide [47]. This relationship corresponded to these nanoparticles being within the motional averaging regime (i.e., on the left side of the curve in Figure 1.7). This correlated well with observations for other MRSw systems [69], and the proposed porous fractal nature of nanoparticle aggregates [60, 61]. Based on these observations, Taktak *et al.* predicted that, as cluster size increases there should be a decrease in the cluster magnetization and increases in the cluster volume fraction [61].

In addition to exploring the fundamental physics that underlie MRSw, Taktak *et al.* introduced some new methods for improving assay performance. The first method consisted of tuning the dynamic range and sensitivity of the assay by

changing the concentration of nanoparticles in solution. For the avidin biosensor, the sensitivity of the T_2 response increased and dynamic range, or the target concentration range over which the biosensor was responsive, decreased at lower nanoparticle concentrations. Conversely, at higher nanoparticle concentrations the sensitivity decreased and the dynamic range increased. This observation indicated that the dynamic range and sensitivity of an assay could be tuned by means of the nanoparticle concentration [61].

The second method introduced by Taktak *et al.* provided a means for controlling nanoparticle precipitation. As discussed in the present and subsequent reports, under certain conditions nanoparticle clusters can become unstable in solution and precipitate [49, 61, 69]. Precipitation, which leads to an increase in T_2, is most often caused by the over-titration of analyte, which leads to extremely large clusters [61, 69]. This may be detrimental to MRSw measurements because, in this case, it leads to a different change in T_2 than would be expected for target-induced clustering. Fortunately, T_1 can be used as an independent marker for particle precipitation, because T_1 depends only on the total amount of soluble iron in solution, and not on the clustering state of the nanoparticles [61]. Taktak *et al.* demonstrated that T_1 remained constant when T_2 changed from analyte-induced nanoparticle clustering, a similar observation to that made for the first MRSw biosensor [1]. Upon over-titration, both the T_2 and T_1 increased, indicating a loss of iron from solution and a shift of the assay conditions to outside the linear response curve. Taktak and coworkers subsequently recommend a workflow to validate that an assay is within the linear response curve by taking both T_2 and T_1 measurements [61]. Although this workflow was initially intended for manual sample preparation, it could be integrated into an automated fluidic handling system for applications that require minimal user interaction.

A third method introduced by Taktak *et al.* was to monitor the coefficient of variation between multiple T_2 measurements, and thus to determine if the biosensor solution was within the linear response range, or if the reagents had precipitated or degraded in some way. It was shown that, when three T_2 measurements were obtained within several minutes, the coefficient of variation between measurements was increased dramatically when particle precipitation or instability had occurred. The utility of this approach was analogous to that of the T_1 measurement system, in that it allowed for an independent verification that the measured T_2 value could be used to obtain the concentration of target via a calibration curve [61]. These methods are important when independently validating the integrity of biosensor measurements.

The methods introduced by Taktak *et al.* were later extended at T2 Biosystems to demonstrate how splitting a sample between multiple nanoparticle reagent chambers could provide validated results, and also expand the biosensor dynamic range [49]. These methods were demonstrated with the same avidin-sensitive biotinylated MRSw architecture. The addition of avidin led to nanoparticle clustering and a change in T_2 from 350 ms to 175 ms. The methods introduced by Taktak *et al.* were extended to include a control for variations in the background T_2, which can be observed in complex samples such as blood due to variations in the

physico-chemical properties that may affect T_2, such as hemoglobin content and viscosity. Sample-to-sample variations could be controlled by splitting the sample between two nanoparticle reagent chambers, such that the detection chamber contained nanoparticles sensitized to the target analyte, while the reference chamber contained identical nanoparticles that were not sensitized to the target analyte. The addition of a sample would then lead to a difference in T_2 between the two chambers only when the analyte was present (Figure 1.11). Accordingly, the calibration curve would be determined from the difference in T_2 between the sample and control chambers [49].

Splitting the sample between multiple chambers can also be used to expand the dynamic range by preloading chambers with different concentrations of nanoparticles. This would allow for higher sensitivity measurements at low target concentrations, and simultaneous lower sensitivity measurements over a much wider dynamic range. In time, this approach will most likely diminish the proportion of inaccurate readings due to biosensor prozoning, and also avoid the user having to prepare sequential dilutions of the sample [49].

These approaches for validating acquired T_2 values can be applied by measuring multiple samples sequentially with a single detector [61], or by acquiring T_2 measurements from two samples simultaneously with a single detector [49]. The T2 Biosystems team demonstrated that a single detection coil could be used to measure the T_2 of two samples at the same time by means of a tailored bi-exponential fit method. This method was shown to accurately measure two T_2 values as long as they were at least 21% different. This approach can also expand the number of simultaneous measurements from a single detection coil, thus increasing the number of possible tests on a given hardware system [49]. However, the

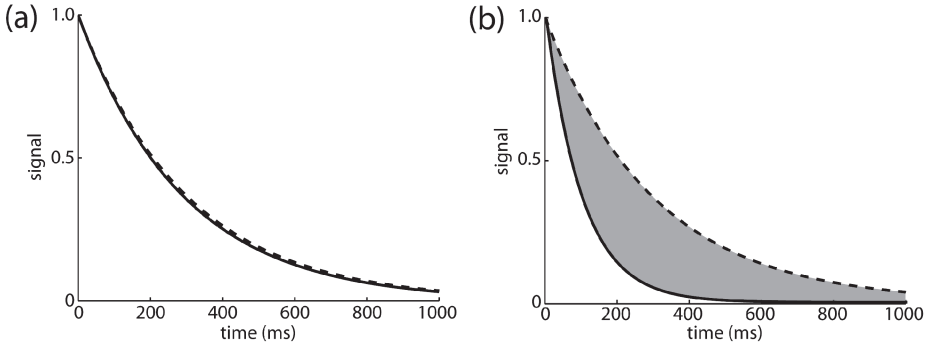

Figure 1.11 Background variations in T_2 can be controlled by splitting the sample between two chambers: one chamber that contains particles sensitized to the target analyte (solid line), and one that contains particles *not* sensitized to the target analyte (dashed line). (a) In the absence of analyte, the two chambers will have identical relaxation curves and no change in T_2 will be reported; (b) In the presence of analyte, the chamber with sensitized nanoparticles will have a different T_2 from that of the reference chamber (shaded area). The quantitative change in T_2 can be obtained by curve fitting [49].

methods for addressing background variations in T_2 and expanding the dynamic range can be applied in a variety of detection coil configurations, including the multiplexed detection hardware introduced by H. Lee in the Weissleder group, which will be discussed in greater detail below [23].

A team led by I. Koh in the Josephson laboratory at MGH has demonstrated that a combination of methods can be used to increase the projected sensitivity of a MRSw assay by five orders of magnitude [19]. The model system used to demonstrate these methods consisted of superparamagnetic nanoparticles or microparticles decorated with the Tag peptide, which is from the HA of the human influenza virus. The addition of an anti-Tag antibody led to clustering of the peptide-decorated particles. The method employed CLIO nanoparticles that were 30 nm in diameter, did not settle, had 20–30 attached peptides per nanoparticles, an R_2 of $50\,s^{-1}\,mM^{-1}$, a magnetization of 86.6 emu g^{-1} Fe, with 8000 iron atoms per nanoparticle, and a concentration of 2.8×10^{-9} for a T_2 of 100 ms. The microparticles used were 1000 nm in diameter, settled less than 5% in aqueous solution [20], had 3×10^5 peptides per particle, an R_2 of $43\,s^{-1}\,mM^{-1}$, a magnetization of $105\,emu\,g^{-1}$ Fe, 2.8×10^9 Fe atoms per particle, and a concentration of 5.1×10^{-15} for a measured T_2 of 100 ms. Koh *et al.* characterized the performance of these nanoparticles in terms of EC_{50} and projected sensitivity. For simplicity, the projected sensitivity will be discussed at this point [19].

When the nanoparticles (NP) and microparticles (MP) were titrated with anti-Tag antibody, the T_2 values decreased for the NP and increased for the MP, which corresponded to the NP being within the motional averaging regime and the MP being within the visit-limited regime [19]. The NP and MP exhibited projected sensitivities of 26 n*M* and 0.41 n*M*, respectively. The >60-fold increase in sensitivity for MP arose from the larger mass of iron per unit conjugated peptide that corresponded to a much larger R_2 relaxivity on a per particle basis [19, 20]. Previous studies with viral targets have suggested that crosslinking agents with a greater binding valency could lead to increased sensitivity [46], and this was confirmed by Koh *et al.*, who increased the valency of their bivalent antibody target to a tetravalent target with the addition of an antibody that selectively bound the Fc region of the anti-Tag antibody. This increased the projected sensitivity for the MP to 0.0002 n*M*, or by a factor of 2000 [19].

The use of MP allows for an additional method for sensitivity enhancement. Investigations conducted by Baudry and coworkers in Paris showed that the reaction rate between reactive groups on magnetic MP could be greatly accelerated by magnetic field-induced self-assembly of the MP into linear chains [21–23] or fractal agglomerates [20]. For Koh *et al.*, an alignment of the magnetic dipoles of individual MP during incubation in a 0.47 T bench-top magnet led to spatial confinement of the MP and increased reaction kinetics. During incubation in the magnet, the T_2 increased due to the linear self-assembly of the MP. In order to distinguish the magnetic-field induced T_2 changes from analyte-induced T_2 changes, the sample was removed from the magnet for a few minutes prior to T_2 measurement. If analyte was present, the MP remained clustered, but if no analyte was present then the MP would disperse due to Brownian motion. This method, termed

magnetic aggregation, resulted in seven- and two-fold increases in projected sensitivity when used with and without valency enhancement, respectively. Magnetic aggregation cannot be applied to NP-based assays due to the attractive forces between the magnetic dipoles of individual NP being much smaller than the forces of Brownian motion [20]. Although it has not been exactly determined, the increase in sensitivity for MP-based assays from magnetic aggregation most likely arose from the more rapid kinetics due to the confinement and resultant close proximity of reactive surfaces. The method of magnetic aggregation has also been applied to solution viscosity measurements by monitoring the rate of change in T_2 over the course of MP aggregation and dispersion phenomena [20].

The most important lesson derived from the findings of Koh *et al*. was that many different methods can be used to increase MRSw sensitivity. For example, Koh *et al*. reported a sensitivity enhancement over the basic NP biosensor configuration of 10^5 due to the use of MP, valency enhancement, and magnetic aggregation. As they showed, many sensitivity enhancement methods are multiplicative in their effect, providing for highly sensitive, tailored results for a given assay. The ideal combination of methods will depend on the particular requirements for a biosensing application, which include reagent stability, time to results, dynamic range, and sensitivity.

1.8 Micro-NMR of Magnetic Relaxation Switch Biosensors

A key component to enabling the successful application of magnetic relaxation switch biosensors is to tailor, in appropriate fashion, the detection platform to the setting in which it will be used. A variety of settings would greatly benefit from a universal detection technology such as MRSw biosensors. These include applications such as biowarfare first responders and home testing, both of which require highly mobile, robust, and perhaps handheld, instruments; applications such as biomarker discovery, which require automation and high throughput; and applications such as health clinics or doctor's offices, which require a compact, user-friendly bench-top unit. Although the majority of commercial magnetic resonance detection instruments are very large, recent progress in magnetic resonance technology engineering has demonstrated scalability and portability. In this section, we will introduce the magnetic readers that have been used to obtain MRSw biosensor measurements, summarize the recent progress in magnetic resonance instrumentation that has enabled the development of miniaturized detectors for biosensor applications, and also provide an update on progress towards developing portable MRSw biosensor readers.

An alternative measurement approach has been proposed to circumvent the low sample measurement throughput of current bench-top systems by a team at MGH, led by D. Hogemann. This group demonstrated the use of a 1.5 T magnetic resonance scanner and T_2-weighted magnetic resonance images to provide HTS for nanoparticle-based reagents. By using this method, up to 1920 samples could be

measured in 50 min by obtaining T_2-weighted spin echo images from each sample in six 384-well plates (only 320 samples per plate were measured due to the limited field of view of the detection coil) [89]. Although other research groups have used this approach to characterize MRSw biosensors, the associated cost for scanner time and challenges in quantitatively relating the T_2 values obtained at 1.5 T to those measured at lower fields will likely limit the widespread use of this approach. A possible high-throughput development platform for MRSw biosensors would consist of a bench-top unit with a throughput of between tens and thousands of samples per hour. This would enable T_2 measurements to be obtained with detector specifications that matched those of portable readers, and also to reduce the associated cost to the level of other bench-top analytical instrumentation.

Recent advances in the field of portable and micro NMR have provided the technological breakthroughs in miniaturized magnetic resonance detectors and magnets for developing truly portable and integrated diagnostic measurement devices. These breakthroughs have included new types of detection coil fabrication methods that allow for submicroliter detection volumes and submillimeter sizes in selenoidal coils that are either hand-wound [90–92] or machine-wound [93, 94]; alternatively, planar detection coils would allow straightforward integration with silicon microchannels [95, 96] and microfluidic systems [97, 98]. Additional breakthroughs have demonstrated that nanoliter volumes can be detected with high sensitivity using microfabricated coils [99–101], and high-sensitivity micro-coils of novel architectures [102].

These advances in miniaturized detection coil design and fabrication have been applied to magnetic resonance instruments with permanent magnets at fields near 0.5 T [103, 104]. Recently, a group at the University of New Mexico and Sandia National Laboratories, led by L. Sillerud, demonstrated the use of a microfabricated detection coil and permanent magnet system for the detection of iron oxide MP [105]. Sillerud *et al*. demonstrated the use of a 550 µm outer diameter solenoidal microcoil (264 nl) in combination with a highly homogeneous (0.06 ppm) 1.04 T permanent magnet (weight > 50 kg) to detect the presence of micron-sized superparamagnetic iron oxide nanoparticles, which are similar to oral-SPIO that are routinely used for magnetic separations. The presence of magnetic particles was detected by detecting a change in the T_2^*, which can be measured via the decay rate of the time domain signal, or by a change in the linewidth of the frequency domain signal [105]. Although the detection of analyte was not demonstrated, it is likely that such systems will be developed for detecting cells that have been tagged with superparamagnetic microparticles. The ultimate aim would be to attain single cell sensitivity by decreasing the size of the detection coil.

A much smaller magnet than that used in the above-described study is currently under development [106], although the use of a CPMG pulse sequence to measure T_2, rather than measuring T_2^*, would inherently allow for measurements in a less uniform magnet, which would be smaller and less expensive. The application of pulse sequences such as CPMG, which enable accurate measurements to be made in highly inhomogeneous magnetic fields, will be critical in allowing magnetic resonance to enter the filed of applications that require low cost and portability.

Recent improvements and optimizations of the CPMG sequence have permitted perhaps the most extreme example of magnetic resonance relaxation measurements in inhomogeneous fields, namely oil well logging, which involves obtaining measurements external to a single-sided magnet and planar detection coil inserted deep within an oil well [107].

In recent years, magnet design technology has progressed to move magnetic resonance measurements outside of the conventional high-field magnet laboratory by creating customized, portable magnets. Many of the current developments in magnetic resonance hardware and methods have been directed towards spectroscopic and imaging measurements that require much higher magnetic field uniformities than the relaxation measurements used for MRSw. The technical advances that result from efforts towards creating portable magnetic resonance spectroscopy and imaging systems will directly benefit MRSws. Other applications that have benefited from such progress include on-site materials characterization [108–114], oil well logging [107], foods analyses [115, 116], portable tendon injury scanning [117], imaging [118–121], and magnetic resonance spectroscopy [122–124] and relaxometry measurements outside of enclosed permanent magnet systems (often referred to as "ex-situ NMR"). Many of these advances have been made with single-sided magnets for the measurement of bulky samples that cannot be fitted within an enclosed permanent magnet assembly [106, 109, 113, 115, 121]. Although such architectures are not directly relevant to most MRSw applications, the fabrication and measurement methods pioneered for these applications will undoubtedly become essential in the design of miniature magnets for diagnostic readers. One example of these advances in magnet hardware, which has directly benefited the development of smaller magnetic resonance instruments, is that of Halbach magnet design [125]. Halbach magnets for magnetic resonance usually consist of multiply oriented discrete magnetic blocks that are used to achieve a single homogeneous "sweet spot" at the region of the magnet occupied by the detection coil. These magnets have been used for both bench-top, single-sided [113, 126] and enclosed [104, 127, 128] magnetic resonance applications.

A team in the Weissleder group has recently demonstrated the use of a downsized magnet, downsized detection coils, and downsized spectrometer components for the detection of MRSws. This team, led by H. Lee, built a 0.49 T relaxometer from a palm-sized magnet and planar microcoils [23], with some of the spectrometer components being integrated onto a printed circuit board (PCB). When using this system, the authors reported an 80-fold increase in mass sensitivity for a MRSw model system. In accordance with microcoil NMR sensitivity improvements of mass-limited samples, this increase in mass sensitivity arose almost entirely from the decrease in detection volume (from ~300 µl to ~5 µl). The absolute sensitivity of the microcoils in terms of the signal-to-noise ratio of the water signal was ~10 after 64 scans, which was much lower than that of commercial bench-top systems [23]. This decreased performance most likely arose from the less efficient planar microcoil detector and less homogeneous magnetic field used in the miniaturized system; by comparison, the commercial bench-top system had a much more sensitive solenoid coil and a more homogeneous magnet.

However, for a given amount of sample, there is an optimal RF microcoil geometry for maximum sensitivity, the optimization of which will most likely allow for these microcoil sensitivity limitations to be overcome. Most importantly, the system built by Lee *et al*. proved to be a powerful demonstration of the portability and ease of use available to MRSw applications.

An additional benefit of miniaturizing the magnetic resonance detection system is a greater multiplexing capability. Because the homogeneous region of a magnet is limited, the smaller volume occupied by microcoils can allow for multiple detection coils within a single magnet. Lee *et al*. utilized this approach by constructing an array of eight microfabricated planar detection coils for their miniaturized magnetic resonance instrument (Figure 1.12a). The eight coils were connected to a single-channel spectrometer by means of a multiplexer switch, and the system was used to detect eight biomarkers from single samples in parallel for both diabetes and cancer biomarker panels (Figure 1.12) [12]. These studies represented a powerful demonstration of how MRSw might provide users with readings for a panel of biomarkers relevant to a specific diagnostic condition, such as cancer. Because of the breadth of the demonstrated target analytes for MRSw, such panels would be capable of spanning an unprecedented range of analyte classes (e.g., cellular, protein, molecular, protein, enzymatic, and therapeutic, etc.), thus yielding a virtually limitless set of test menus for specific applications.

Whilst the studies of H. Lee elegantly demonstrated the potential for downsized detection coils and magnets for MRSw biosensors [23], a subsequent and complementary effort by the team of Y. Liu *et al*. at Harvard, in the laboratory of Donhee

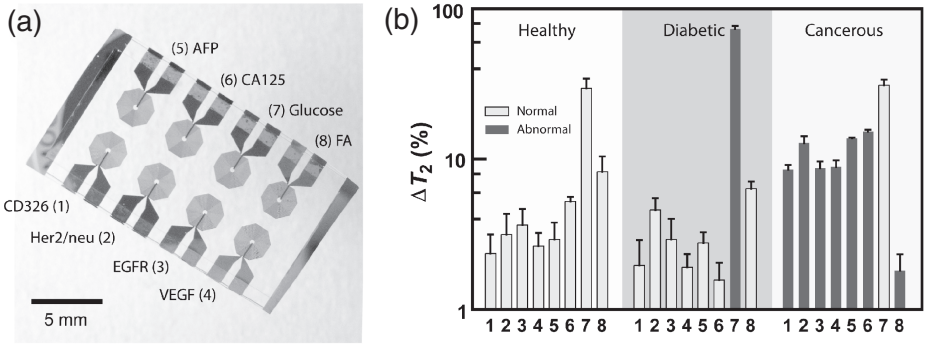

Figure 1.12 Demonstration of MRSw multiplexing by means of microcoils. (a) A planar microcoil array of eight detection coils fabricated from electroplated copper on a glass substrate. Each microcoil was positioned under a sample well containing nanoparticles sensitized to a different analyte; (b) Spiked serum samples representing diabetic or cancer sera were analyzed by aliquoting the sample between the detection coils and measuring the change in T_2 relative to normal sera. This approach demonstrated the potential of MRSw for monitoring multiple biomarkers from a single sample simultaneously [23]. This figure was a generous gift from Dr Hakho Lee, Center for Systems Biology, Massachusetts General Hospital, Boston, MA.

Ham, demonstrated the capability of significantly downsizing the spectrometer. Although, prior to the studies of Y. Liu *et al*., single PCB spectrometers had been demonstrated [129–131], in order for MRSw biosensor detectors to achieve the size, cost, and range of applications of conventional portable electronics, it was necessary to downsize the entire magnetic resonance spectrometer to the scale of an integrated circuit (IC). The studies of Liu *et al*. represented the most significant steps towards achieving this, by showing that the heart of a spectrometer – the transceiver – could be hosted on an IC. The CMOS design of Liu *et al*. was able to transmit and receive RF pulses to and from a detection coil [132], although a similar performance was reported (in terms of sensitivity) to that achieved by Lee *et al*. with a transceiver built from off-the-shelf, discrete components. The RF transceiver of Liu *et al*. has proved to be one of the smallest transceiver units reported to date [132]. The integration of other spectrometer components should enable an extremely small complete magnetic resonance spectrometer.

These breakthroughs in magnetic resonance detection instrumentation suggest that this technology can be tailored to biosensor applications that require downsized and portable readers. In fact, efforts are currently under way at T2 Biosystems to produce completely integrated, portable MRSw biosensor readers that would most likely consist of a relaxometer (magnet, detection coil, and spectrometer) as well as a user interface, power source, and connection to external data networks. Depending on the application, the MRSw biosensor reader may also provide sample incubation, disposable cartridge reading and handling, and fluidics actuation. Recently, a team from T2 Biosystems, led by P. Prado, introduced a shoebox-sized, fully integrated relaxometer that weighs less than 4 kg [73], and consists of a 0.5 T magnet, spectrometer, operating system, touchscreen user interface, and DC power input. Additional investigations at T2 Biosystems have demonstrated the capability of further downsizing a 0.5 T magnet unit to be 10 000-fold smaller than a commercial bench-top magnet and probehead units [73], by means of an extremely low-cost magnet and coil architecture. Moreover, when using this prototype magnet and microcoil, MRSw biosensor-mediated measurements of hCG protein were conducted at femtomolar levels, in nanoliter sample volumes. Due to the range of application of these MRSw biosensor tests, and the recent and ongoing breakthroughs in the downsizing of instruments, continued development will in time surely enable the deployment of MRSw biosensors within virtually any setting, and for virtually any target.

Acknowledgments

The author acknowledges the T2 Biosystems team and expresses his gratitude to those who provided helpful feedback for this chapter, including Lee Josephson, Sonia Taktak, Hakho Lee, Pablo Prado, Vicky Demas, Kim Foster, and Sonia Kumar. The author also acknowledges the many hours of relinquished time from Sherri, Sophia, and Henry Lowery.

References

1 Josephson, L., Perez, J.M. and Weissleder, R. (2001) Magnetic nanosensors for the detection of oligonucleotide sequences. *Angewandte Chemie, International Edition in English*, **40**, 3204–6.

2 Perez, J.M., Josephson, L. and Weissleder, R. (2004) Use of magnetic nanoparticles as nanosensors to probe for molecular interactions. *Chembiochem*, **5**, 261–4.

3 Li, W.-H., Fraser, S.E. and Meade, T.J. (1999) A calcium-sensitive magnetic resonance imaging contrast agent. *Journal of the American Chemical Society*, **121**, 1413–14.

4 Loui, A.Y., Huber, M.M., Ahrens, E.T., Rothbacher, U., Moats, R., Jacobs, R., Fraser, S.E. and Meade, T.J. (2000) In vivo visualization of gene expression using magnetic resonance imaging. *Nature Biotechnology*, **18**, 321–5.

5 Aime, S., Botta, M., Eliana, G. and Terreno, E. (2000) A p(O2)-responsive MRI contrast agent based on the redox switch of manganese(II/III)-porphyrin complexes. *Angewandte Chemie, International Edition in English*, **39**, 747–50.

6 Nivorozhkin, A.L., Kolodzieg, A.F., Caravan, P., Greenfield, M.T., Lauffer, R.B. and McMurry, T.J. (2001) Enzyme-activated Gd^{3+} magnetic resonance imaging contrast agents with a prominent receptor-induced magnetization enhancement. *Angewandte Chemie, International Edition in English*, **40**, 2903–6.

7 Hanaoka, K., Kikuchi, K., Urano, Y., Narazaki, M., Yokawa, T., Sakamoto, S., Yamaguchi, K. and Nagano, T. (2002) Design and synthesis of a novel magnetic resonance imaging contrast agent for selective sensing of zinc ion. *Chemistry & Biology*, **9**, 1027–32.

8 Aime, S., Castelli, D.D. and Terreno, E. (2002) Novel pH-reporter MRI contrast agents. *Angewandte Chemie, International Edition in English*, **41**, 4334–6.

9 Aime, S., Castelli, D.D., Fedeli, F. and Terreno, E. (2002) A paramagnetic MRI-CEST agent responsive to lactate concentration. *Journal of the American Chemical Society*, **124**, 9364–5.

10 De Leon-Rodriguez, L.M., Ortiz, A., Weiner, A.L., Zhang, S., Kovacs, Z., Kodadeck, T. and Sherry, A.D. (2002) Magnetic resonance imaging detects a specific peptide-protein binding agent. *Journal of the American Chemical Society*, **124**, 3514–15.

11 Lowery, T.J., Rubin, S.M., Ruiz, E.J., Spence, M.M., Winssinger, N., Schultz, P.G., Pines, A. and Wemmer, D.E. (2003) Applications of laser-polarized ^{129}Xe to biomolecular assays. *Magnetic Resonance Imaging*, **21**, 1235–9.

12 Schroeder, L., Lowery, T.J., Hilty, C., Wemmer, D.E. and Pines, A. (2006) Molecular imaging using a targeted magnetic resonance hyperpolarized biosensor. *Science*, **314**, 446–9.

13 Gilchrist, R.K., Medal, R., Shorey, W.D., Hanselman, R.C., Parrott, J.C. and Taylor, C.B. (1957) Selective inductive heating of lymph nodes. *Annals of Surgery*, **146**, 596–606.

14 Thorek, D.L., Chen, A.K., Czupryna, J. and Tsourkas, A. (2006) Superparamagnetic iron oxide nanoparticle probes for molecular imaging. *Annals of Biomedical Engineering*, **34**, 23–8.

15 Pankhurst, Q.A., Conolly, J., Jones, S.K. and Dobson, J. (2003) Applications of magnetic nanoparticles in biomedicine. *Journal of Physics D: Applied Physics*, **36**, R167–81.

16 Josephson, L., Bigler, J. and White, D. (1991) The magnetic properties of some materials affecting MR images. *Magnetic Resonance in Medicine*, **22**, 204–8.

17 Jung, C.W. (1995) Surface properties of superparamagnetic iron oxide MR contrast agents: ferumoxides, ferumoxtran, ferumoxsil. *Magnetic Resonance Imaging*, **13**, 675–91.

18 Josephson, L., Lewis, J., Jacobs, P., Hahn, P.F. and Stark, D.D. (1988) The effects of iron oxides on proton relaxivity. *Magnetic Resonance Imaging*, **6**, 647–53.

19 Koh, I., Hong, R., Weissleder, R. and Josephson, L. (2008) Sensitive NMR sensors detect antibodies to influenza. *Angewandte Chemie, International Edition in English*, **47**, 4119–21.

20 Hong, R., Cima, M.J., Weissleder, R. and Josephson, L. (2008) Magnetic microparticle aggregation for viscosity determination by MR. *Magnetic Resonance in Medicine*, **59**, 515–20.

21 Baudry, J., Rouzeau, C., Goubault, C., Robic, C., Cohen-Tannoudji, L., Koenig, A., Bertrand, E. and Bibette, J. (2006) Acceleration of the recognition rate between grafted ligands and receptors with magnetic forces. *Proceedings of the National Academy of Sciences of the United States of America*, **103**, 16076–8.

22 Cohen-Tannoudji, L., Bertrand, E., Baudry, J., Robic, C., Goubault, C., Pellissier, M., Johner, A., Thalmann, F., Lee, N.K., Marques, C.M. and Bibette, J. (2008) Measuring the kinetics of biomolecular recognition with magnetic colloids. *Physical Review Letters*, **100**, 108301.

23 Lee, H., Sun, E., Ham, D. and Weissleder, R. (2008) Chip-NMR biosensor for detection and molecular analysis of cells. *Nature Medicine*, **14**, 869–74.

24 Jung, C.W., Weissleder, R., Josesphson, L., Bengele, H. and Brady, T.J. (1996) Physical properties of MION-46 and AMI-27, Presented at the Society of Magnetic Resonance Fourth Scientific Meeting, New York, 1996.

25 Jung, C.W. and Jacobs, P. (1995) Physical and chemical properties of superparamagnetic iron oxide MR contrast agents: ferumoxides, ferumoxtran, ferumoxsil. *Magnetic Resonance Imaging*, **13**, 661–74.

26 Josephson, L., Groman, E.V., Menz, E., Lewis, J.M. and Bengele, H. (1990) A functionalized superparamagnetic iron oxide colloid as a receptor directed MR contrast agent. *Magnetic Resonance Imaging*, **8**, 637–46.

27 Weissleder, R., Elizondo, G., Wittenburg, J., Rabito, C.A., Bengele, H.H. and Josephson, L. (1990) Ultrasmall superparamagnetic iron oxide: characterization of a new class of contrast agents for MR imaging. *Radiology*, **175**, 489–93.

28 Whitesides, G.M., Kazlauskas, R.J. and Josephson, L. (1983) Magnetic separations in biology. *Trends in Biotechnology*, **1**, 144–8.

29 Franzred, M., Siemann-Herzberg, M., Hobley, T.J. and Thomas, O.R. (2006) Protein purification using magnetic adsorbent particles. *Applied Microbiology and Biotechnology*, **70**, 505–16.

30 Shen, T., Weissleder, R., Papisov, M., Bogdanov, A. and Brady, T.J. (1993) Monocrystalline iron oxide nanocompounds (MION): physiochemical properties. *Magnetic Resonance in Medicine*, **29**, 599–604.

31 Weissleder, R., Lee, A.S., Fischman, A.J., Reimer, P., Tueng, S., Wilkinson, R., Callahan, R. and Brady, T.J. (1991) MR antibody imaging: polyclonal human IgG labelled with polymeric iron oxide. *Radiology*, **181**, 245–9.

32 Weissleder, R., Bogdanov, A. and Papisov, M. (1992) Drug targeting in magnetic resonance imaging. *Magnetic Resonance Quarterly*, **8**, 55–63.

33 Weissleder, R., Lee, A.S., Khaw, A., Shen, T. and Brady, T.J. (1992) Antimyosin-labeled monocrystalline iron oxide allows detection of myocardial infarct: MR antibody imaging. *Radiology*, **182**, 381–5.

34 Tartaj, P., Morales, M.D.P., Veintemillas-Verdaguer, S., Gonzalez-Carreno, T. and Serna, C.J. (2003) The preparation of magnetic nanoparticles for applications in biomedicine. *Journal of Physics D: Applied Physics*, **36**, R182–97.

35 Jun, Y.-W., Lee, J.-H. and Cheon, J. (2008) Chemical design of nanoparticle probes for high-performance magnetic resonance imaging. *Angewandte Chemie, International Edition in English*, **47**, 5122–35.

36 Park, J., An, K., Hwang, Y., Park, J.-G., Noh, H.-J., Kim, J.-Y., Park, J.-H., Hwang, N.-M. and Hyeon, T. (2004) Ultra-large-scale synthesis of monodisperse nanocrystals. *Nature Materials*, **3**, 891–5.

37 Laurent, S., Forge, D., Port, M., Roch, A., Robic, C., Van der Elst, L. and Muller, R.N. (2008) Magnetic iron oxide nanoparticles: synthesis, stabilization, vectorization, physiochemical characterizations, and biological applications. *Chemical Reviews*, **108**, 2064–110.

38 Gupta, A.K. and Gupta, M. (2005) Synthesis and surface engineering of iron oxide nanoparticles for biomedical applications. *Biomaterials*, **26**, 3995–4021.

39 Petri-Fink, A. and Hofmann, H. (2007) Superparamagnetic iron oxide nanoparticles (SPIONs): from synthesis to in vivo studies–a summary of the synthesis, characterization, in vitro, and in vivo investigations of SPIONs with particular focus on surface and colloidal properties. *IEEE Transactions on Nanobioscience*, **6**, 289–97.

40 Wunderbaldinger, P., Josephson, L. and Weissleder, R. (2002) Crosslinked iron oxides (CLIO): a new platform for the development of targeted MR contrast agents. *Academic Radiology*, **9** (Suppl. 2), S304–6.

41 Josephson, L., Tung, C.-H., Moore, A. and Weissleder, R. (1999) High-efficiency intracellular magnetic labeling with novel superparamagnetic-tat peptide conjugates. *Bioconjugate Chemistry*, **10**, 186–91.

42 Singer, J.M. and Plotz, C.M. (1956) The latex fixation test. I. Application to the serologic diagnosis of rheumatoid arthritis. *The American Journal of Medicine*, **21**, 888–92.

43 Price, C.P. and Newman, D.J. (1997) *Principles and Practice of Immunoassay*, MacMillan Reference, London.

44 Van Weemen, B.K. and Shuurs, A.H.W. (1971) Immunoassay using antigen-enzyme conjugates. *FEBS Letters*, **15**, 232–6.

45 Perez, J.M., Josephson, L., O'Loughlin, T., Högemann, D. and Weissleder, R. (2002) Magnetic relaxation switches capable of sensing molecular interactions. *Nature Biotechnology*, **20**, 816–20.

46 Perez, J.M., Simeone, F.J., Saeki, Y., Josephson, L. and Weissleder, R. (2003) Viral-induced self-assembly of magnetic nanoparticles allows the detection of viral particles in biological media. *Journal of the American Chemical Society*, **125**, 10192–3.

47 Zhao, M., Josephson, L., Tang, Y. and Weissleder, R. (2003) Magnetic sensors for protease assays. *Angewandte Chemie, International Edition in English*, **42**, 1375–8.

48 Kaittanis, C., Naser, S.A. and Perez, J.M. (2007) One-step, nanoparticle-mediated bacterial detection with magnetic relaxation. *Nano Letters*, **7**, 380–3.

49 Lowery, T.J., Palazzolo, R., Wong, S.M., Prado, P.J. and Taktak, S. (2008) Single-coil, multisample, proton relaxation method for magnetic relaxation switch assays. *Analytical Chemistry*, **80**, 1118–23.

50 Hahn, E.L. (1950) Nuclear induction due to free Lamour precession. *Physical Review*, **77**, 297–8.

51 Carr, H.Y. and Purcell, E.M. (1954) Effects of diffusion on free precession in nuclear magnetic resonance experiments. *Physical Review*, **94**, 630–8.

52 Meiboom, S. and Gill, D. (1958) Modified spin-echo method for measuring nuclear relaxation times. *Review of Scientific Instruments*, **29**, 688–91.

53 Muller, R.N., Gillis, P., Moiny, F. and Roch, A. (1991) Transverse relaxivity of particulate MRI contrast media: from theories to experiments. *Magnetic Resonance in Medicine*, **22**, 178–82.

54 Weisskoff, R.M., Zuo, C.S., Boxerman, J.L. and Rosen, B.R. (1994) Microscopic susceptibility variation and transverse relaxation: theory and experiment. *Magnetic Resonance in Medicine*, **31**, 601–10.

55 Bulte, J.W.M., Brooks, R.A., Moskowitz, B.M., Bryant, L.H. and Franck, J.A. (1998) T1 and T2 relaxometry of monocrystalline iron oxide nanoparticles (MION-46L): theory and experiment. *Academic Radiology*, **5** (Suppl. 1), S137–40.

56 Brooks, R.A. (2002) T2-shortening by strongly magnetized spheres: a chemical exchange model. *Magnetic Resonance in Medicine*, **47**, 388–91.

57 Gillis, P., Moiny, F. and Brooks, R.A. (2002) On T2-shortening by strongly magnetized sphere: a partial refocusing model. *Magnetic Resonance in Medicine*, **47**, 257–63.

58 Brooks, R.A., Moiny, F. and Gillis, P. (2001) On T2-shortening by weakly magnetized particles: the chemical exchange model. *Magnetic Resonance in Medicine*, **45**, 1014–20.

59 Shapiro, M.G., Atanasijevic, T., Faas, H., Westmeyer, G.G. and Jasanoff, A. (2006) Dynamic imaging with MRI contrast agents: quantitative considerations. *Magnetic Resonance Imaging*, **24**, 449–62.

60 Atanasijevic, T., Shusteff, M., Fam, P. and Jasanoff, A. (2006) Calcium-sensitive MRI contrast agents based on superparamagnetic iron oxide nanoparticles and calmodulin. *Proceedings of the National Academy of Sciences of the United States of America*, **103**, 14707–12.

61 Taktak, S., Sosnovik, D., Cima, M.J., Weissleder, R. and Josephson, L. (2007) Multiparameter magnetic relaxation switch assays. *Analytical Chemistry*, **79**, 8863–9.

62 Roch, A., Gossuin, Y., Muller, R.N. and Gillis, P. (2005) Superparamagnetic colloid suspensions: water magnetic relaxation and clustering. *Journal of Magnetism and Magnetic Materials*, **293**, 532–9.

63 Tsourkas, A., Hofstetter, O., Hofstetter, H., Weissleder, R. and Josephson, L. (2004) Magnetic relaxation switch immunosensors detect enantiomeric impurities. *Angewandte Chemie, International Edition in English*, **43**, 2395–9.

64 Perez, J.M., O'Loughlin, T., Simeone, F.J., Weissleder, R. and Josephson, L. (2002) DNA-based magnetic nanoparticle assembly acts as a magnetic relaxation nanoswitch allowing screening of DNA-cleaving agents. *Journal of the American Chemical Society*, **124**, 2856–7.

65 Sun, E.Y., Weissleder, R. and Josephson, L. (2006) Continuous analyte sensing with magnetic nanoswitches. *Small*, **2**, 1144–7.

66 Grimm, J., Perez, J.M., Josephson, L. and Weissleder, R. (2004) Novel nanosensors for rapid analysis of telomerase activity. *Cancer Research*, **64**, 639–43.

67 Park, I.-K., Ng, C.-P., Wang, J., Chu, B., Yuan, C., Zhang, S. and Pun, S.H. (2008) Determination of nanoparticle vehicle unpackaging by MR imaging of a T2 magnetic relaxation switch. *Biomaterials*, **29**, 724–32.

68 Harris, T.J., von Maltzahn, G., Derfus, A.M., Ruoslahti, E. and Bhatia, S.N. (2006) Proteolytic actuation of nanoparticle self-assembly. *Angewandte Chemie, International Edition in English*, **45**, 3161–5.

69 Kim, G.Y., Josephson, L., Langer, R. and Cima, M.J. (2007) Magnetic relaxation switch detection of human chorionic gonadotrophin. *Bioconjugate Chemistry*, **18**, 2024–8.

70 Daniel, K.D., Kim, G.Y., Vassiliou, C.C., Jalili-Yazdi, F., Langer, R. and Cima, M.J. (2007) Multi-reservoir device for detecting a soluble cancer biomarker. *Lab on a Chip*, **7**, 1288–93.

71 Atanasijevic, T. and Jasanoff, A. (2008) Preparation of iron oxide-based calcium sensors for MRI. *Nature Protocols*, **2**, 2582–9.

72 Taktak, S., Weissleder, R. and Josephson, L. (2008) Electrode chemistry yields a nanoparticle-based sensor for calcium. *Langmuir*, **24**, 7596–8.

73 Lowery, T.J., Demas, V. and Prado, P.J. (2008) Portable and implantable magnetic resonance based molecular diagnostics, oral presentation 49th ENC 2008, March, 9–14, Pacific Grove, CA.

74 Kumar, S., Mozeleski, B., Wong, S., Taktak, S., Lowery, T.J. and Foster, K. Particles 2008. Magnetic relaxation diagnostics using superparamagnetic nanoparticles, May 2008, Orlando, FL. Available at: http://www.nanoparticles.org/Particles2008/.

75 Perez, J.M., Simeone, F.J., Tsourkas, A., Josephson, L. and Weissleder, R. (2004)

Peroxidase substrate nanosensors for MR imaging. *Nano Letters*, **4**, 119–22.

76 Bil, I., Rybka, B. and Wozniak, M. (2008) Adenoviral infection–pathomechanism and diagnostics. *Advances in Clinical and Experimental Medicine*, **17**, 91–9.

77 Spencer, J.V., Newcomb, W.W., Thomsen, D.R., Homa, F.L. and Brown, J.C. (1998) Assembly of the herpes simplex virus capsid: preformed triplexes bind to the nascent capsid. *Journal of Virology*, **72**, 3944–51.

78 Olson, J., Ishikawa, F., Rowan, M. and Sallinen, J. (2006) Performance of the anemia panel assays (ferritin, folate and vitamin B12) on the Abbott AxSYM® instrument. American Association of Clinical Chemistry meeting, July 23–27, Chicago, Illinois. Available at: http://www.abbottdiagnostics.es/ciencia/pdf/18.pdf.

79 Moss, M.W., Carella, A.V., Provost, V. and Quinn, T.C. (1996) Comparison of absolute CD4+ lymphocyte counts determined by enzyme immunoassay (TRAx CD4 test kit) and flow cytometry. *Clinical and Diagnostic Laboratory Immunology*, **3**, 371–3.

80 Reynolds, F., O'Loughlin, T., Weissleder, R. and Josephson, L. (2005) Method of determining nanoparticle core weight. *Analytical Chemistry*, **77**, 814–17.

81 Högemann, D., Josephson, L., Weissleder, R. and Basilon, J.P. (2000) Improvement of MRI probes to allow efficient detection of gene expression. *Bioconjugate Chemistry*, **11**, 941–6.

82 Sun, E.Y., Josephson, L., Kelly, K.A. and Weissleder, R. (2006) Development of nanoparticle libraries for biosensing. *Bioconjugate Chemistry*, **17**, 109–13.

83 Sun, E.Y., Josephson, L. and Weissleder, R. (2006) "Clickable" nanoparticles for targeted imaging. *Molecular Imaging*, **5**, 122–8.

84 Hermanson, G.T. (1996) *Bioconjugate Techniques*, Academic Press, San Diego.

85 Montet, X., Funovics, M., Montet-Abou, K., Weissleder, R. and Josephson, L. (2006) Multivalent effects of RGD peptides obtained by nanoparticle display. *Journal of Medicinal Chemistry*, **49**, 6087–93.

86 Schellenberger, E.A., Reynolds, F., Weissleder, R. and Josephson, L. (2004) Surface-functionalized nanoparticle library yields probes for apoptotic cells. *ChemBioChem*, **5**, 275–9.

87 Weissleder, R., Kelly, K., Sun, E.Y., Shtatland, T. and Josephson, L. (2005) Cell-specific targeting of nanoparticles by multivalent attachment of small molecules. *Nature Biotechnology*, **23**, 1418–23.

88 Weissleder, R., Moore, A., Mahmood, U., Bhorade, R., Benveniste, H., Chiocca, E.A. and Basilon, J.P. (2000) In vivo MR imaging of transgene expression. *Nature Medicine*, **6**, 351–5.

89 Högemann, D., Ntziachristos, V., Josephson, L. and Weissleder, R. (2002) High throughput magnetic resonance imaging for evaluating targeted nanoparticle probes. *Bioconjugate Chemistry*, **13**, 116–21.

90 Wu, N., Peck, T.L., Webb, A.G. and Sweedler, J. (1994) 1H NMR spectroscopy on the nanoliter scale for static and on-line measurements. *Analytical Chemistry*, **66**, 3849–57.

91 Wu, N., Peck, T.L., Webb, A.G., Magin, R.L. and Sweedler, J. (1994) Nanoliter volume sample cells for 1H NMR: application to on-line detection in capillary electrophoresis. *Journal of the American Chemical Society*, **116**, 7929–30.

92 Olson, D.L., Lacey, M.E., Webb, A.G. and Sweedler, J. (1999) Nanoliter-volume 1H NMR detection using periodic stopped-flow capillary electrophoresis. *Analytical Chemistry*, **71**, 3070–6.

93 Olson, D.L., Peck, T.L., Webb, A.G., Magin, R.L. and Sweedler, J.V. (1995) High-resolution microcoil 1H-NMR for mass-limited, nanoliter-volume samples. *Science*, **270**, 1967–70.

94 Seeber, D.A., Hoftiezer, J.H., Daniel, W.B., Rutgers, M.A. and Pennington, C.H. (2000) Triaxial magnetic field gradient system for microcoil magnetic resonance imaging. *Review of Scientific Instruments*, **71**, 4263.

95 Massin, C., Vincent, F., Homsy, A., Ehrmann, K., Boero, G., Besse, P.-A.,

Daridon, A., Verpoorte, E., de Rooij, N.F. and Popovic, R.S. (2003) Planar microcoil-based microfluidic NMR probes. *Journal of Magnetic Resonance*, **164**, 242–55.

96 Sorli, B., Chateaux, J.F., Pitaval, M., Chahboune, H., Favre, B., Briguet, A. and Morin, P. (2004) Micro-spectrometer for NMR: analysis of small quantities in vitro. *Measurement Science and Technology*, **15**, 877–80.

97 Trumbull, J.D., Glasgow, I.K. and Beebe, D.J. (2000) Integrating microfabricated fluidic systems and NMR spectroscopy. *IEEE Transactions on Biomedical Engineering*, **47**, 3–7.

98 Wensink, H., Hermes, D.C. and van den Berg, A. (2004) High signal to noise ratio in low field NMR on chip, simulations and experimental results. 17th IEEE International Conference on Micro Electro Mechanical Systems, Maastricht, Netherlands, January 25–29, pp. 407–10.

99 Peck, T.L., Magin, R.L., Kruse, J. and Feng, M. (1994) NMR microspectroscopy using 100 μm planar RF coils fabricated on gallium arsenide substrates. *IEEE Transactions on Biomedical Engineering*, **41**, 706–9.

100 Stocker, J.E., Peck, T.L. and Webb, A.G. (1997) Nanoliter volume, high-resolution NMR microspectroscopy using a 60-μm planar microcoil. *IEEE Transactions of Biomedical Engineering*, **44**, 1122–7.

101 Massin, C., Boero, G., Vincent, F., Abenhaim, J., Besse, P.-A. and Popovic, R.S. (2002) High-Q factor RF planar microcoils for micro-scale NMR spectroscopy. *Sensors and Actuators A*, **A97–A98**, 280–8.

102 Walton, J.H., de Ropp, J.S., Shotov, M.V., Goloshevsky, A.G., McCarthy, M.J., Smith, R.L. and Collins, S.D. (2003) A micromachined double-tuned NMR Microprobe. *Analytical Chemistry*, **75**, 5030–6.

103 Goloshevsky, A.G., Walton, J.H., Shutov, M.V., de Ropp, J.S., Collins, S.D. and McCarthy, M.J. (2005) Development of low field nuclear magnetic resonance microcoils. *Review of Scientific Instruments*, **76**, 024101.

104 Demas, V., Herberg, J.L., Malba, V., Bernhardt, A., Evans, L., Harvey, C., Chinn, S., Maxwell, R. and Reimer, J. (2007) Portable, low-cost NMR with laser-lathe lithography produced microcoils. *Journal of Magnetic Resonance*, **189** (1), 121–9.

105 Sillerud, L.O., McDowell, A.F., Adolphi, N.L., Serda, R.E., Adams, D.P., Vasile, M.J. and Alam, T.M. (2006) 1H NMR Detection of superparamagnetic nanoparticles at 1 T using a microcoil and novel tuning circuit. *Journal of Magnetic Resonance*, **181**, 181–90.

106 Demas, V., Herberg, J.L., Malba, V., Bernhardt, A., Evans, L., Harvey, C., Chinn, S., Maxwell, R., Franck, J., Reimer, J. and Pines, A. (2008) Ex Situ NMR with microcoils, poster presentation 49th ENC March 9–14, 2008, Pacific Grove, CA.

107 Allen, D., Flaum, C., Ramakrishnan, T.S., Fairhurst, D., Pritchard, T., Bedford, J., Gubelin, G., Heaton, N., Minh, C.C., Ramamoorthy, R., Castelijns, K., Norville, M.A. and Seim, M.R. (2000) Trends in NMR logging. *Oilfield Review*, **12**, 2–19.

108 Blümich, B., Blümler, P., Eidmann, G., Guthausen, A., Haken, R., Schmitz, U., Saito, K. and Zimmer, G. (1998) The NMR-mouse: construction, excitation, and applications. *Magnetic Resonance Imaging*, **16**, 479–84.

109 Eidmann, G., Savelsberg, R., Bluemler, P. and Bluemich, B. (1996) The NMR MOUSE, a mobile universal surface explorer. *Journal of Magnetic Resonance, Series A*, **122**, 104–9.

110 Marko, A., Wolter, B. and Arnold, W. (2007) Application of a portable nuclear magnetic resonance surface probe to porous media. *Journal of Magnetic Resonance*, **185**, 19–27.

111 McDonald, P.J., Aptaker, P.S., Mitchell, J. and Mulheron, M. (2007) A unilateral NMR magnet for sub-structure analysis in the built environment: the surface GARField. *Journal of Magnetic Resonance*, **185**, 1–11.

112 Glover, P.M., Aptaker, P.S., Bowler, J.R., Ciampi, E. and McDonald, P.J. (1999) A novel high-gradient permanent magnet

for the profiling of planar films and coatings. *Journal of Magnetic Resonance*, **139**, 90–7.

113 Prado, P.J. (2001) NMR hand-held moisture sensor. *Magnetic Resonance Imaging*, **19**, 505–8.

114 Manz, B., Coy, A., Dykstra, R., Eccles, C.D., Hunter, M.W., Parkinson, B.J. and Callaghan, P.T. (2006) A mobile one-sided NMR sensor with a homogeneous magnetic field: the NMR-MOLE. *Journal of Magnetic Resonance*, **183**, 25–31.

115 Martin, D.R., Ablett, S., Pedersen, H.T. and Mallett, M.J.D. (2002) The NMR MOUSE: its applications to food science. Special Publication – Royal Society of Chemistry, Magnetic Resonance in Food Science, Vol. **286**, pp. 54–61.

116 Nordon, A., McGill, C.A. and Littlejohn, D. (2001) Process NMR spectrometry. *Analyst*, **126**, 260–72.

117 Haken, R. and Blumich, B. (2000) Anisotropy in tendon investigated in vivo by a portable NMR scanner, the NMR-MOUSE. *Journal of Magnetic Resonance*, **144** (2), 195–9.

118 Rahmatallah, S., Li, Y., Seton, H.C., Mackenzie, I.S., Gregory, J.S. and Aspden, R.M. (2005) NMR detection and one-dimensional imaging using the inhomogeneous magnetic field of a portable single-sided magnet. *Journal of Magnetic Resonance*, **173**, 23–8.

119 Casanova, F., Robert, H., Perlo, J. and Pusiol, D. (2003) Echo-planar rotating-frame imaging. *Journal of Magnetic Resonance*, **162**, 396–401.

120 Rokitta, M., Rommel, E., Zimmermann, U. and Haase, A. (2000) Portable nuclear magnetic resonance imaging system. *Review of Scientific Instruments*, **71**, 4257–62.

121 Prado, P.J. (2003) Single sided imaging sensor. *Magnetic Resonance Imaging*, **21**, 397–400.

122 Perlo, J., Demas, V., Casanova, F., Meriles, C.A., Reimer, J., Pines, A. and Bluemich, B. (2005) High-resolution NMR spectroscopy with a portable single-sided sensor. *Science*, **308**, 1279.

123 Perlo, J., Casanova, F. and Blümich, B. (2007) Ex situ NMR in highly homogeneous fields: 1H spectroscopy. *Science*, **315**, 1110–12.

124 Meriles, C., Sakellariou, D., Henrike, H., Moule, A.J. and Pines, A. (2001) Approach to high-resolution ex situ NMR spectroscopy. *Science*, **293**, 82–5.

125 Halbach, K. (1980) Design of permanent multipole magnets with oriented rare earth cobalt material. *Nuclear Instruments and Methods*, **169**, 1–10.

126 Marble, A.E., Mastikhin, I.V., Colpitts, B.G. and Balcom, B.J. (2007) A compact permanent magnet array with a remote homogenous field. *Journal of Magnetic Resonance*, **186**, 100–4.

127 Moresi, G. and Magin, R. (2003) Miniature permanent magnet for table-top NMR. *Concepts in Magnetic Resonance Part B (Magnetic Resonance Engineering)*, **19B** (1), 35–43.

128 Hills, B.P., Wright, K.M. and Gillies, D.G. (2003) A low-field, low-cost Halbach magnet array for open-access NMR. *Journal of Magnetic Resonance*, **175**, 336–9.

129 Takeda, K. (2008) OPENCORE NMR: open-source core modules for implementing an integrated FPGA-based NMR spectrometer. *Journal of Magnetic Resonance*, **192**, 218–29.

130 Takeda, K. (2007) A highly integrated FPGA-based nuclear magnetic resonance spectrometer. *Review of Scientific Instruments*, **78**, 033103.

131 Job, C., Pearson, R.M. and Brown, M. (1994) A personal computer-based nuclear magnetic resonance spectrometer. *Review of Scientific Instruments*, **65**, 3354–62.

132 Liu, Y., Sun, N., Lee, H., Weissleder, R. and Ham, D. (2008) CMOS mini nuclear magnetic resonance system and its application for biomolecular sensing. *IEEE International Solid-State Circuits Conference*, **7** (3), 140.